

# **MODIFIED VERSION**

**Projektmodul der Mathematisch-  
Naturwissenschaftlichen Fakultät**

**der EBERHARD KARLS UNIVERSITÄT TÜBINGEN  
im Fach Biochemie**

**Schoger, Constantin,  
under Sebastian Wolf**

# 1 Materials and Methods

## 1.1 Plant Material

*Arabidopsis thaliana* sterilized seeds sprinkled onto 1/2MS plate (+0.7% Agar, +1% sucrose; 45 mL for squared petri dish and 30 mL for cell culture dishes), vernalized (10°C, 1-2 days; 1 day for all plates but Col-0 on normal medium), grown in a growth chamber (polyklima, L3-TDL+rF; True Daylight PLUS Weiß-LED, 4000K color temperature, 60% humidity, 22°C). After a certain time (noted in each experiment) the plants were either fixed and cleared or kept in a cold room (10°C) until they were imaged. Stained growth media (either PI or calcofluor white) was prepared by directly weighing the amount into the hot liquified media. Exception to this were the 1.4  $\frac{\mu\text{g}}{\text{mL}}$  and 14  $\frac{\mu\text{g}}{\text{mL}}$  calcofluor white plates. For these a calcofluor white stock solution of 7  $\frac{\text{mg}}{\text{mL}}$  in distilled water was used to pipette the required amount into the media. Additionally for these two calcofluor white plates 0.8% agar was used.

We have made use of an *Arabidopsis* Col-0 line expressing mCherry specifically to the plasma membrane of epidermal tissue (ML1p::mCherry-RCI2A), generously given to us by Margot Smit ([Smit et al. 2023](#)). Thus, this line can be used as a marker for pavement cells in cotyledons.

## 1.2 Fixation and Clearing

Fixation and clearing were performed following a paper ([Ursache et al. 2018](#)). Plants were fixed in cell strainers placed in 6 well plates using 4% PFA (*para*-formaldehyde) in 1x PBS covering the plants under vakuum (dessicator,  $\approx$  100 mbar, 1 h). To reduce surface tension of plants placed in the solution, the plants were gently pressed into the fixation solution using forecepts. After fixation, the material was washed (2x, 1xPBS, 1 min, 32 rpm) and cleared using ClearSee (32 rpm). After a few days, the solution was exchanged. The material was stored in ClearSee (32 rpm) until usage. For repeating fixation and clearing of Col-0 the same plants stored at 10°C were taken (2 months old).

## 1.3 Staining

Cleared samples were stained overnight using calcofluor white (0.1% dissolved in ClearSee), washed (2x, ClearSee,  $\approx$  20 min) and imaged. Imaging was performed on the same day as the fluorescent marker quickly decreases in intensity in ClearSee.

Fresh tissue was imaged with calcofluor white and propidium iodide (PI). Calcofluor white staining (0.1% calcofluor white) was performed under vakuum (dessicator,  $\approx$  100 mbar, 2 h) and washed (1x dH<sub>2</sub>O, 30 min, 32 rpm) in cell strainers in 6 well plates. PI staining, for either cut off cotyledons or whole plants, was performed for 20-40 min in a 1.5 mL reaction tube and washed (1x, dH<sub>2</sub>O, few minutes) while being occasionally shaken using a finger (both for stain and wash).

## 1.4 Microscopy

Imaging was performed on both confocal microscopes (Leica SP8 upright and inverted) and a widefield epifluorescent microscope (Keyence BZ-X810). Using widefield microscopy, fixed and

cleared tissue stained with calcofluor white was imaged using the BZ-X filter DAPI (OP-87762, ex = (360/40) nm, em = (460/50) nm, 400 nm dichroic mirror wavelength) while fresh tissue stained with PI was imaged with the BZ-X filter TexasRed (OP-87765, ex = (560/40) nm, em = (630/75) nm, 585 nm dichroic mirror wavelength). Images were recorded in 14 bit with low photobleach mode on. For stacks the brightness was auto-adjusted using the Keyence capture software at the slide where most pavement cell were in the plane.

Confocal microscopy was used to image calcofluor white (405 nm diode laser, em = 415-500 nm), PI (514 nm argon laser, em = 550-650 nm) or mCherry (561 nm DPPS laser and for 25x dipping at the upright SP8 552 nm DPPS laser, em = 575-650 nm) using a PMT (gain = 600-800, typically 650) or HyD (100%). Images scanned using a Galvano scanner, the resolution was 1024x1024 px in 16 bit and the pinhole was put to 1 AU (440 nm for calcofluor white, 620 nm for PI or mCherry). The laser strength varied, but was typically between 10-30% for PI and mCherry and 0.1-5% for calcofluor white. No line averaging was used.

For inverted imaging (widefield and confocal imaging besides dipping-imaging) an imaging chamber slide was used. For fresh tissue 10-20  $\mu\text{L}$  distilled water was dropped onto the slide and the cotyledon placed onto with its upper epidermis facing downwards towards the objective lens. Fixed and cleared cotyledons were placed from 6 well plate containing ClearSee onto the slide. The attached liquid was often enough, otherwise more was supplemented. Cleared tissue was imaged in three different ways. Either nothing, a 15x15 mm glass slide, or an agar block (gently pressed with a finger) weighed onto the cotyledon. For fresh tissue analyzed with the 25x-dip-cf objective a circular growth plate was flooded with distilled water and analyzed.

Objectives are abbreviated: MMx-y-ZZ, MMx: magnification (e.g. 63x); y: immersion (w: water, g:glycerol), dry, dip (dipping); ZZ: wf (widefield) or cf (confocal).

**Table 1: Objective List.**

| Abbreviation | Description   | NA   |
|--------------|---|------|
| 10x-dry-cf   | 10x dry (confocal, inverted SP8)                    | 0.30 |
| 20x-w-cf     | 20x water-immersed (confocal, inverted SP8)         | 0.70 |
| 63x-w-cf     | 63x water-immersed (confocal, inverted SP8)         | 1.20 |
| 63x-g-cf     | 63x glycerol-immersed (confocal, inverted SP8)      | 1.30 |
| 25x-dip-cf   | 25x water-dipping (upright confocal, SP8)           | 0.90 |
| 20x-dry-wf   | 20x dry (inverted widefield, keyence)               | 0.75 |
| 40x-dry-wf   | 40x dry (inverted widefield, keyence)               | 0.95 |
| 60x-oil-wf   | 60x glycerol-immersed (inverted widefield, keyence) | 1.40 |

## 1.5 Image Manipulation

We used MorphoGraphX ([Strauss et al. 2021](#)) (Version 2.0r1-246 on a Win11 machine) to display stacks as 3D images and clip through the tissue. Most MorphoGraphX images in this thesis were adjusted. Specifically, in MorphoGraphX the main stack's transfer function as well its opacity were adjusted to reveal the region or problem of interest. This was especially done for the mCherry-expressing line as the upper and lower part of the cell walls were faint.

Further, the images of the media-stained cotyledons (Figure 10, Figure 11) were, manipulated using Fiji's (Schindelin et al. 2012) (Version 2.14.0/1.54f with Java 1.8.0\_322 (64-bit) on a Win11 machine) *enhance contrast* function using a value of 0.35 and applying normalization. This has been done as as the original images were practically not visible by eye when zoomed out.

## 1.6 Image Processing

To process images, we made use of Fiji, MorphoGraphX and PaCeQuant (Möller et al. 2017) (MiToBo Version 2.3.1), a tool developed specifically for PC segmentation. The various projections using only Fiji without MorphoGraphX were performed to the six cotyledons according to the following Fiji macro. Note that you need to redefine the *series* variable for each cotyledon. Otherwise, the images will be overwritten.

```

1 series = "003"
2 //simple max-z-projection
3 run("Z Project...", "projection=[Max Intensity]");
4 run("Flip Vertically");
5 saveAs("Tiff", "D:/MorphoGraph/Confocal/062524/Margot_6dag_20x/No_Morpho/n6/MAX_"+series+
    "_HyD_.tif");
6
7 //max-z-projection -> subtract-bg
8 run("Subtract Background...", "rolling=1");
9 saveAs("Tiff", "D:/MorphoGraph/Confocal/062524/Margot_6dag_20x/No_Morpho/n6/MAX_subtract-bg-
    rolling1_"+series+"_HyD_.tif");
10 close()
11
12 //subtract-bg -> max-z-projection
13 run("Subtract Background...", "rolling=1 stack");
14 run("Z Project...", "projection=[Max Intensity]");
15 run("Flip Vertically");
16 saveAs("Tiff", "D:/MorphoGraph/Confocal/062524/Margot_6dag_20x/No_Morpho/n6/subtract-bg-
    rolling1_MAX_"+series+"_HyD_.tif");
17 close("*");

```

For all PaCeQuant segmentations the same settings were used: Phase to run = SEGMENTATION\_AND\_FEATURES, Batch mode, Pixel calibration mode = AUTO, Border Contrast = BRIGHT\_ON\_DARK, Segmentation Algorithm = SEGMENTATION ANISOTROPIC FILTERS, Heuristic for Gap Closing = WATERSHED, Gaussian Sigma Interpolation = PHYSICALSIZE, Niblack threshold = 4.0, Spine Length Interpretation = ABSOLUTE, Maximal spine length = 40.0, Branch Points in Spines = DISALLOWED, Minimal Size of Cells = 500.0, Maximal Size of Cells = 100000.0, Unit for Size Thresholds = MICRONS, Draw region IDs to output images = TRUE.

The genereal MorphoGraphX workflow is described in Figure 5. First, we loaded the stack. Note that you may need to apply Stack/Canvas/ReverseAxes (x=y=no, z=yes) after loading the stack as it may be up side down. Applying the gaussian filter (Stack/Filters/GaussianBlurStack, x=y=z) is dependent on the applied worfklow. It is abbreviated as gX (e.g. g3 for gaussian of x=y=z=3). Afterwards, Stack/Morphology/EdgeDetect is applied to get the foundation for creating the surface. Here, we only change one parameter, the threshold (abbreviated as TXXXX, e.g. T1000 for a threshold of 1000). The other parameters are Multiplier = 2.0, AdaptFactor = 0.3, FillValue = 30000. Normally, the surface is created next but in one workflow we first filled holes (Stack/Morphology/FillHoles) for which we never changed any parameter

but rather applied it multiple times (X-Radius = Y-Radius = 10, Threshold = 10000, Depth = 0, Fill Value = 30000). Mesh/Creation/MarchingCubeSurface creates the surface. We have not change the Threshold of 5000, but did change the cube size once. Unless otherwise stated, it equals 5.0. The surface is then smoothed (Mesh/Structure/SmoothMesh) and subdivided (Mesh/Structure/Subdivide) once each. Next, in order to project the original signal, the main stack is loaded as the work stack (Stack/MultiStack/CopyMainToWorkStack). Afterwards, the stack is annihilated everywhere but in a certain range of distance towards the surface (normal vector) via Stack/MeshInteraction/Annihilate. The constant parameters for this thesis are Fill=No and FillVal=30000. We describe the minimal and the maximal distance parameters as XX-YY (e.g. 10-14, i.e. annihilate everything but 10-14  $\mu\text{m}$  from the surface). Finally, the work stack has to be loaded as the main stack (Stack/MultiStack/CopyWorkToMainStack) and saved via the Stack1/save button on the top left of the GUI.

We then loaded the new stack into Fiji. Here we faced two problems: the annihilation function also included signal from the edges and from the bottom. To get rid of the bottom signal, as it will disturb the projection, we went through the stack until we didnt see any evenly spread signal across the whole image anymore, duplicated the stack from the slice after the bottom-signal up to the end. Finally, still using Fiji we created a MAX-z-projection and saved it as a tif file, afterwich we ran PaCeQuant on it.

## 1.7 Segmentation Error Quantification

Errors were recorded manually by counting them against the respective projection, or a projection of the same stack if said projection yielded a poor projection. Segmentaions were subdivided into cut-offs, over-segmentations, under-segmentations and no-segmentation. Cut-off errors can occur either seemingly random (as depicted in Figure 3C) or because of a border not in the correct plane (Figure 3D). If there is a cut-off at the edge of the image with the edge directly cutting the cell at one side it is not counted as an error as it is likely due to the edge. Over-segmentations are cells divided into two or more segmentations. Under-segmentaion is defined as a cell being consumed by a neighbouring one, i.e. there should have been another segmentation. Under-segmentations mostly occurred with stomata being completely or partially consumed. One cell may have multiple of said errors either of the same type or different errors in/at the same cell. In this case all errors are counted. No-segmentation describes the occurrence of pavement cells not on the edge of the cell that are not being segmented. This only applies to cells not at the edge as we have used the function of PaCeQuant to not segment any cells that are not as a whole visible. Note that because of the edge problem of the MorphoGraphX workflow there are many cells that do get segmented at the edge as it has a signal. This is not counted as an error as this is due to the edge. Additionally, a cell is only counted as non-segmented if it is also big enough, i.e a typical pavement cell and not a small cell adjacent to stomata guard cells. Examples for the different error types can be found in Figure 3. Please take these error counts with a grain of salt as it can be quite subjective when to label something as an error in certain cases.

In order to compare segmentation quality between stacks the total number of errors is divided by the number of (corrected) cells yielding  $e_{pc}$ . The number of (corrected) cells equals the amount of cells separated by PaCeQuant subtracted with the amount of over-segmentations (Equation 1).

The amount of under-segmented cells are not added as mostly stomata, which should not be segmented in the first place, are consumed by other cells. However, a cell consuming part of another cell or another cell completely can occur. However, this metric ought to be enough to convey the total amount of errors roughly.

$$e_{pc} = \frac{\# \text{errors}}{\# \text{cells} - \# \text{oversegmentations}} \quad (1)$$

To compare the different workflows we use the mean of six cotyledon stacks as well as their standard deviation (SD).

## 1.8 Chemicals

**Table 2: Chemical List.** In the case of two products being listed it was not noted which one was used for which batch.

| Chemical                                     | Company           | Product Nr.         |
|--|-------------------|---------------------|
| MS Medium (+Vitamins)                        | Duchefa Biochemie | M0256.0050          |
| Phyto Agar                                   | Duchefa Biochemie | P1003.1000          |
| Sucrose                                      | not noted         |                     |
| Ethanol                                      | Sigma-Aldrich     | 32221-2.5L-M        |
| NaOCl  | not noted         |                     |
| Para-formaldehyde                            | ROTH              | 0964.3              |
| Calcofluor White (Fluorescent Brightener 28) | MP Biomedicals    | 02158067-CF         |
| Urea   | Sigma-Aldrich     | U5128-1KG           |
|  | Riedel-de Haen    | 33247 (2.5 kg)      |
| Xylitol                                      | Sigma-Aldrich     | W507940-1KG         |
| Sodium Deoxycholate                          | Sigma Aldrich     | D6750-25G           |
|  | Sigma Aldrich     | D6750-500G          |
| Propidium Idodie                             | ROTH              | CN74.1              |
| PBS  | not noted         |                     |
| Glycerol                                     | not noted         |                     |
| Immersol 518 F                               | ZEISS             | 4Y00-R0DY-1007-3VF3 |

## 1.9 Materials

**Table 3: Material List.** In the case of two products being listed it was not noted which one was used for which batch.

| Material           | Company         | Product Nr. |
|--------------------|-----------------|-------------|
| cell culture dish  | greiner BIO-ONE | 664160      |
| petri dish, square | greiner BIO-ONE | 688102      |
| 6 well plates      | greiner BIO-ONE | 657160      |
| cell strainers     | corning         | 431752      |

|                              |                 |            |
|------------------------------|-----------------|------------|
| filter 0.22um                | ROTH            | KH54.1     |
| 1 mL syringe                 | BRAUN           | 9166017V   |
| cover slips 15x15 mm         | not noted       |            |
| chambers slides              | ibidi           | 80287      |
| 1.5 mL safe seal tubes       | SARSTEDT        | 72.690.001 |
| 2 mL safe seal tubes         | SARSTEDT        | 72.691     |
| 2 mL safe seal tubes (brown) | SARSTEDT        | 72.691.001 |
| 50 mL falcon tubes           | SARSTEDT        | 62.547.254 |
|                              | greiner BIO-ONE | 227261     |

---

## 2 Results

### 2.1 Fresh Tissue or Fixed and Cleared Tissue

Using inversed confocal microscopy we sought to analyze fixed and cleared as well as fresh *Arabidopsis* cotyledon pavement cells (PCs). After recording z-stacks using 63x objectives their 3D structure was analyzed using MorphoGraphX (Strauss et al. 2021). The PCs of fresh tissue (Figure 1A) mostly showed a regularly curved cell surface. However, some cells were pressed flat at the top. Cleared and fixed tissue (Figure 1B-D) showed irregular shapes. Placing the cotyledon on the slide with nothing on top (Figure 1B), as in the case of fresh tissue, resembled the native shape of fresh PCs (Figure 1A). However, upon closer inspection the cell surface was not smooth, rather it was folded and uneven. When placing a cover slip as weight on the cotyledons back, it was pressed flat similar to the flat PCs in fresh tissue (Figure 1A). However, this flatness is in stark contrast to the even flatness of fresh tissue, as it folded in various places. As a cover slip appears to press the cotyledon too much, an agar block was put on the cotyledons back and gently pressed on with a finger (Figure 1D). While the shape resembled the one of fresh tissue, it was once again folded.

As it is important that the cell borders are well defined we investigated the folded structures further by clipped through the stack (Figure 2). Fresh tissue recorded with a 20x objective showed regularly defined cell borders (Figure 2A-B). In the case of the 63x stack of fresh tissue clipping revealed defined borders with some PCs flat on the top, as already observed in Figure 1A. In contrast to this, fixed and cleared tissue showed more or less irregular cell borders as well as the folded surfaces (Figure 2D-H). As we will describe at a later point, the current workflow for segmentation requires the extraction of the cell surface using MorphoGraphX in order to account for curved tissue and cell surfaces. Folded structures, as we have observed in cleared and fixed tissue, present a challenge for said surface extraction. Figure 2G shows that the fold was not accurately captured when creating a mesh (surface) with the usually used  $5\text{ }\mu\text{m}$  *cube size* parameter. Even when going down to  $0.5\text{ }\mu\text{m}$  *cube size* this did not change while simultaneously increasing the processing time from a few minutes to several hours per stack.

Note that the images of fixed and cleared tissue was taken approximately 2 months after fixation. To test whether the strange shapes were due to the tissue being stored for too long in ClearSee solution, the experiment was repeated for tissue kept for only one month in ClearSee (Figure S2) and about a week in ClearSee (Figure S3). Both looked the same compared to two months after clearing in regards to being folded. We also applied the later touched upon workflow to the cleared and fixed tissue. Here, the 2 month cleared tissue using nothing to weight the cotyledon down resulted in an odd result where the stack was annihilated in a weird manner Figure S1. This was repeated for the 1 month cleared tissue where the workflow did not yield this issueFigure S3B.

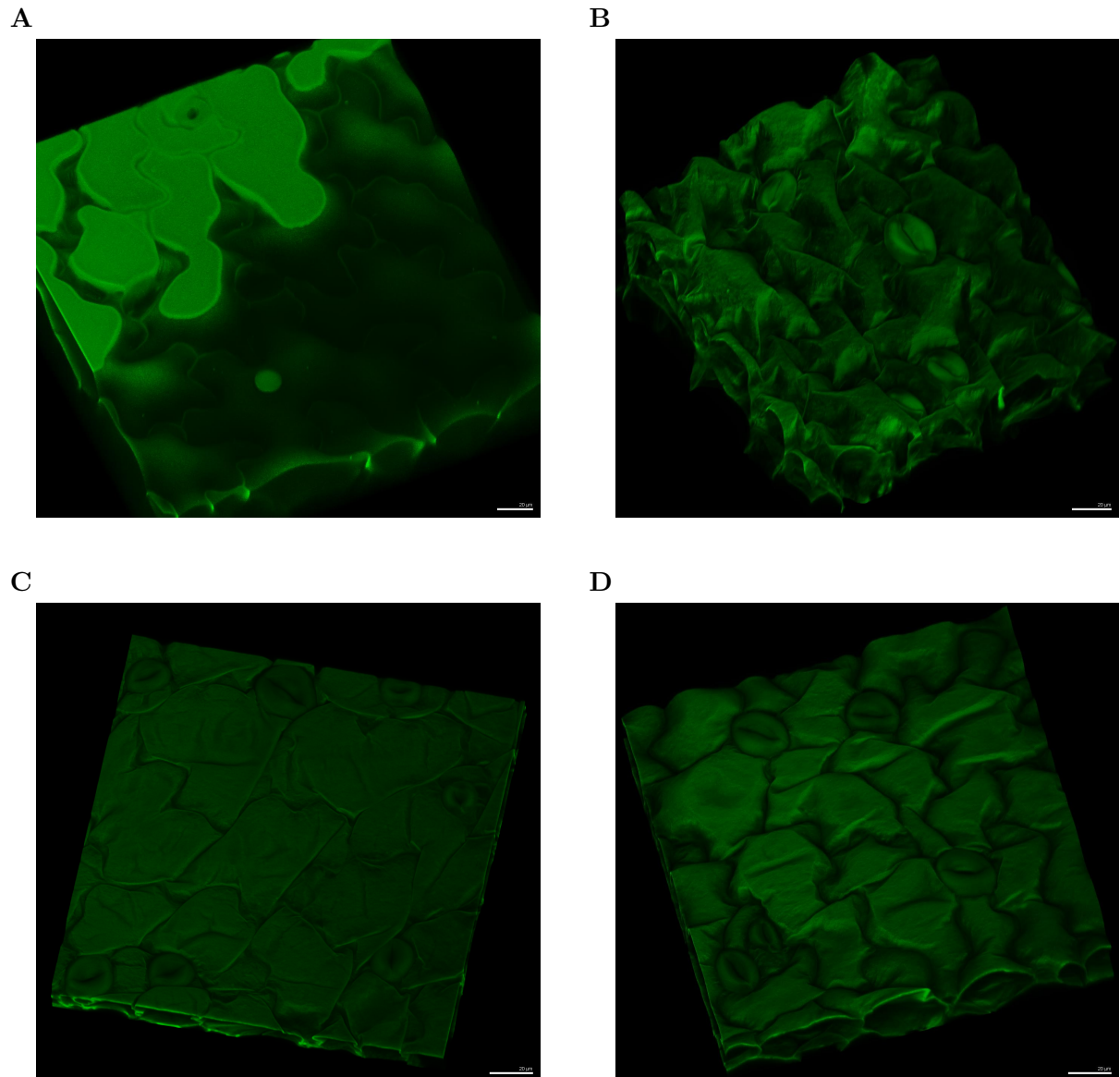


**Figure 1:** 3D depictions of 7day-old fresh tissue vs fixed and cleared tissue in MorpheoGraphX. (A) Fresh PI-stained cotyledon captured with 63x water-immersion objective, confocal (63x-w-conf). (B-D) Fixed and cleared calcofluor white stained cotyledons captured with 63x glycerol-immersion objective, confocal (63x-g-conf). Nothing (B), 15x15 mm glass cover slip (C) and agar block (D) placed on top of cotyledon's back. Scale bars: 20  $\mu$ m

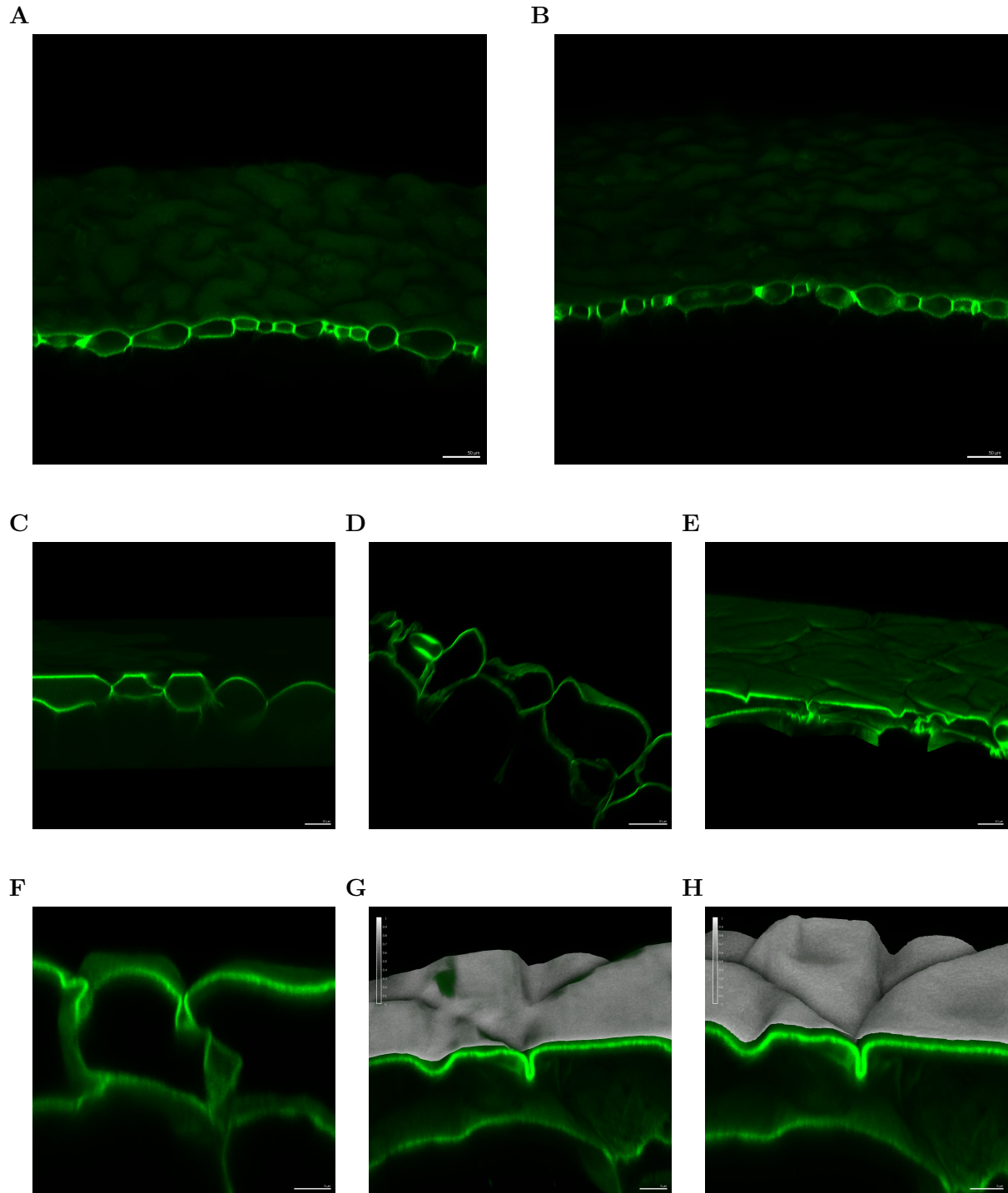


**Figure 2: Clips through the 3D depiction of cleared tissue in MorphoGraphX.** (A-B) Fresh tissue of line expressing mCherry specifically to the plasma membrane of its epidermal cells; 20x water-immersion objective, confocal (20x-w-conf). (C-H) Clips through the tissue of the 3D images from Figure 1. (C) Fresh PI-stained tissue; 63x-w-conf. (D-F) Fixed and cleared calcofluor white stained of nothing, slide and agar placed on the cotyledon's back, respectively; 63x-g-conf. (G-H) Close-up of fold including the cell surface of cleared and fixed cotyledon with agar on its back. Projected surface (white) using 0.3 Gaussian filter (G0.3), edge detect threshold of 5000 (T5000), marching cube size of 5  $\mu\text{m}$  (M5)(G) or 0.5  $\mu\text{m}$  (M0.5)(H), 1x smoothed (1xS), 1x annihilated (1xA). Scale bars: (A-B): 50  $\mu\text{m}$ ; (C-D): 20  $\mu\text{m}$ ; (E): 10  $\mu\text{m}$ ; (F-H): 5  $\mu\text{m}$ .

## 2.2 The Problem of Curvature and Non-Uniform Cell Thickness

Here we seek to employ PaCeQuant (Möller et al. 2017), a watershed-based segmentation tool developed specifically for pavement cells. As not all cell borders are in one plane, which is especially true for fresh tissue, we decided to record z-stacks of the cotyledons of an *Arabidopsis* line expressing mCherry only in the plasma membrane of epidermal tissue and tried to project them into one plane. For this, we employed a maximum projection using Fiji (Schindelin et al. 2012). In the projection the cells were well distinguishable by eye, however the inside of the cells were not clean as the underlying parenchyma cells, likely visible due to autofluorescence, is also projected (Figure 3A). Applying PaCeQuant-segmentation resulted in many segmentation errors (Figure 3B). These include seemingly random cut-offs (Figure 3C) as well as cut-offs due to a cell border not in plane (Figure 3D), over-segmentation (Figure 3E), under-segmentation (Figure 3F and Figure 3G) which are mostly related to stomata, and no segmentation where there should be one (Figure 3H). Note that cells not completely in frame are supposed to not be segmented. We quantified the different errors which in total amounted to 40.57% errors per (corrected) cell  $e_{pc}$  (as defined in Materials and Methods) (Table 4). As we assumed the background as part of the problem, we applied a rolling background subtraction of pixel size one both after projection (Figure 4A-B), and before projection onto each slide separately (Figure 4c-D). This resulted in an  $e_{pc}$  of 38.14% and 41.41%, respectively.

**Table 4: Errors for non-MorphoGraphX attempts.** Counts of different error types, total number of errors (#errors), amount of cells detected by PaCeQuant segmentation (#cells) as well as the amount of errors per (corrected) cell  $e_{pc}$  for a max-z-projection (MAX), a max-z-projection followed by a rolling background subtraction of one pixel (MAX-bg-substr) and the rolling background subtraction (one px) applied onto the whole stack before max-z-projection.

| Projection    | # cells | # errors  | cut-offs | overseg | underseg | no seg | $e_{pc}$ |
|---------------|---------|-----------|----------|---------|----------|--------|----------|
| MAX           | 126     | <b>43</b> | 14       | 20      | 8        | 1      | 40.57%   |
| MAX-bg-substr | 107     | <b>37</b> | 7        | 10      | 20       | 0      | 38.14%   |
| bg-substr-MAX | 117     | <b>41</b> | 13       | 18      | 19       | 1      | 41.41%   |

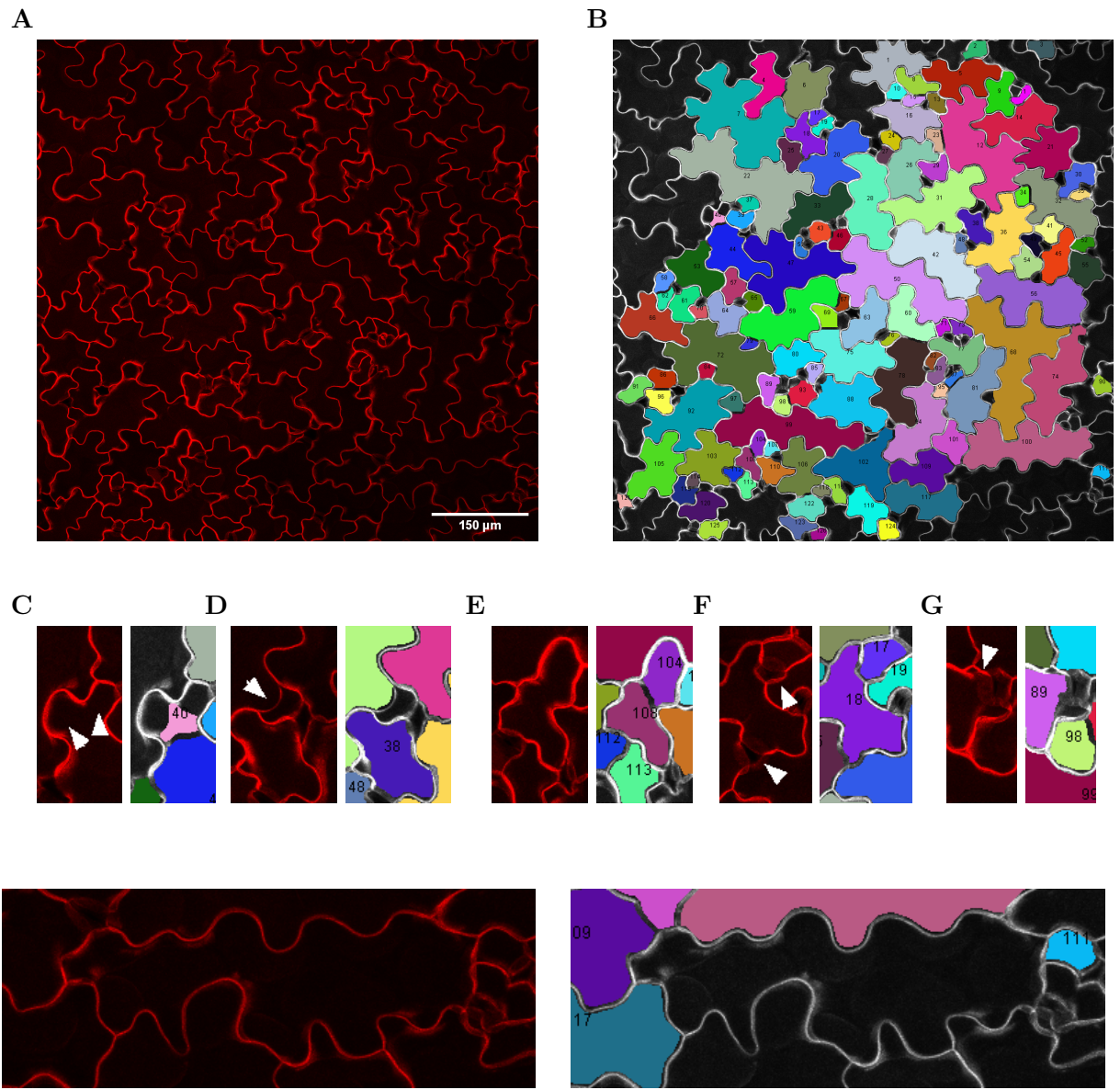


**Figure 3: Segmentation of MAX-z-projection.** (A) MAX-z-projection of cotyledon (01); 20x-wcf. (B) Colored result from PaCeQuant on (A). (C-H) Examples for segmentation error classes, on the left the projection (white arrows may show region of interest) and on the right the segmentation: (C) cut-off cell, seemingly random; (D) cut-off cell, due to cell border not being in the correct plane; (E) over-segmentation of one cell; (F) under-segmentation, one cell completely consumed another; (G) under-segmentation, one cell partially consumed another; (H) no segmentation.

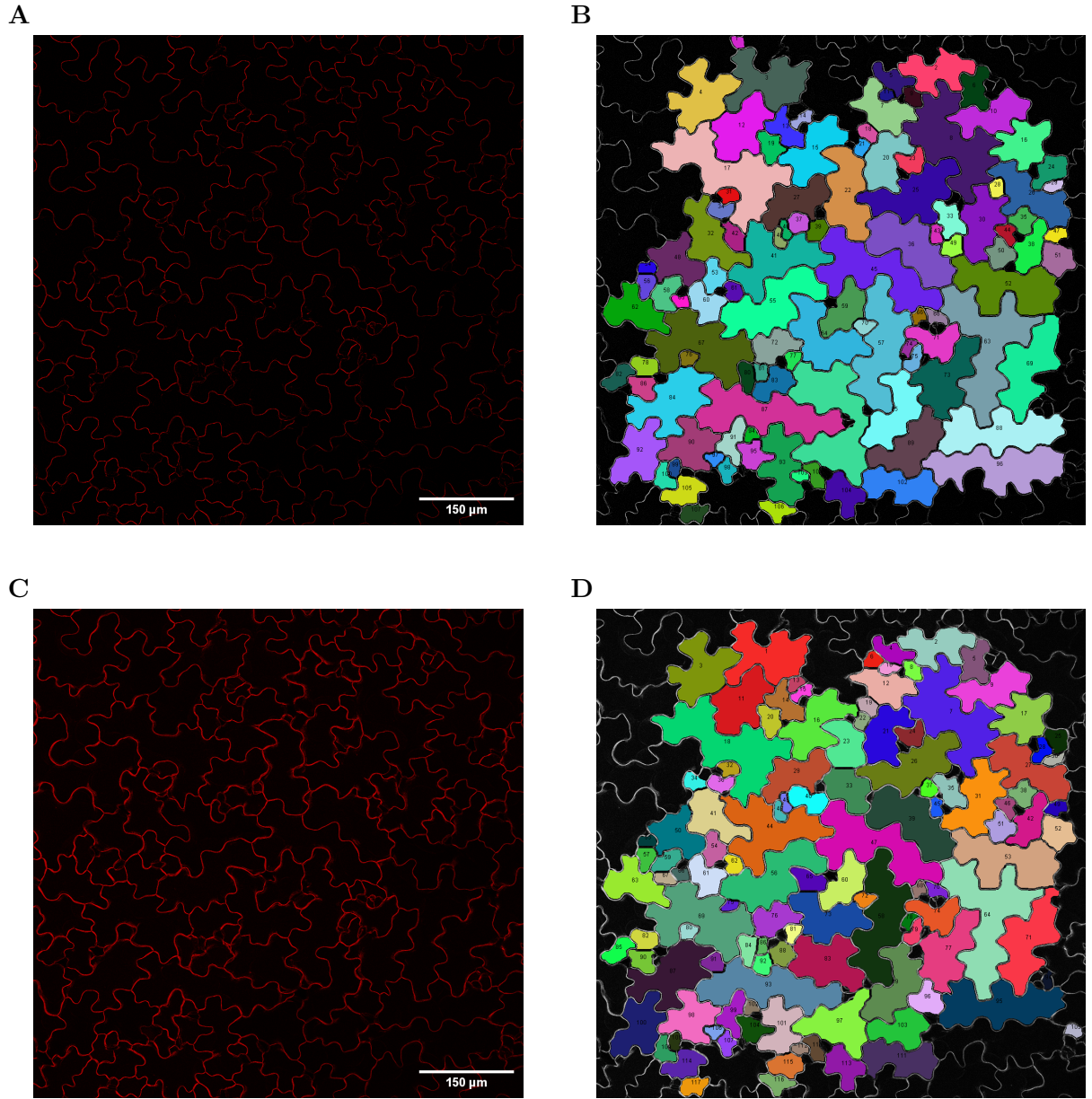


**Figure 4: Segmentation of MAX-z-projection with background subtraction.** (A) MAX-z-projection and rolling background subtraction of pixel size one of cotyledon (01); 20x-w-cf. (B) Colored result from PaCeQuant on (A). (C) rolling background subtraction of pixel size one before MAX-z-projection of cotyledon (01); 20x-w-cf. (D) Colored result from PaCeQuant on (B).

To combat the curvature, the likely reason for the prior results, we sought to adapt a workflow extracting the surface of the stack and projecting only signal in a certain distance to each point of the surface Erguvan et al. 2019. The workflow makes use of MorpoGraphX (Strauss et al. 2021), a tool commonly used for segmentation of tissue. In MorphographX the stack is loaded (Figure 5A), a Gaussian filter is applied (Figure 5B), edges of the stack are detected (Figure 5C) and a surface (aka mesh) is created, smoothed and subdivided (Figure 5D). Finally, the original, un-Gaussian signal is only kept at a certain distance to the surface using the *Annihilate* function (Figure 5E). The resulting stack is then loaded into Fiji, projected (MAX) (Figure 5F) and fed to PaCeQuant (Figure 5G). Note that we faced an issue where the annihilation occurred from all directions of the surface resulting in edges in the stack (Figure 5F) as well as signal at the bottom. The signal at the bottom, being one to a few slices thick depending on the annihilation, was removed by only using the stack after the slice of signal (not shown).

In regards to parameter tuning the most important ones were the size of the Gaussian filter, the threshold for edge detection and the distance projected from the surface in the *Annihilation* function. Two issues that arose were noise being detected as part of the surface, which we call *peaks*, (Figure 6A-B) and the surface not being detected which created holes in the surface (Figure 6C-D). The former issue was typically due to too low thresholds in edge detection and could also be combated using a higher Gaussian filter. The latter was due to a low threshold in edge detection. Thus, it was crucial to keep the threshold low enough to not see peaks, but high enough to not introduce holes into the surface. Using a Gaussian filter of  $0.3\text{ }\mu\text{m}$  and an edge detect threshold of 2000 (G0.3T2000 workflow) resulted in no holes and an average amount of peaks (Figure 6A-B). As we had concerns about the peaks, we opted to rather use a Gaussian filter of  $1\text{ }\mu\text{m}$ , which still had some small peaks, instead of a Gaussian filter of  $0.3\text{ }\mu\text{m}$  as well as a threshold of 1000 (G1T1000). Using this, we wanted to test the workflow using the same mCherry marked plants as before to get an idea of the error-rate. For this, we had recorded six cotyledons of individual plants 6dag. Note that the first cotyledon "01" is the same one used for the prior attempts with no surface extraction (Figure 3, Figure 4). Using this cotyledon (01) we first tried different annihilation distances in order to figure out which we would use for the whole series of cotyledons (Table S1). As none were perfect segmentations we decided to use the best three for all cotyledons. These were  $12 - 14\text{ }\mu\text{m}$  with an  $e_{pc}$  of 0.89%,  $10 - 12\text{ }\mu\text{m}$  with  $e_{pc} = 2.75\%$  and  $10 - 14\text{ }\mu\text{m}$  with  $e_{pc} = 2.68\%$  (Table S1). Applying these values onto all six cotyledons resulted in a mean of 6.80% ( $SD=4.68\%$ ), 6.99% ( $SD=5.10\%$ ) and 7.84% ( $SD=4.55\%$ ) for  $10 - 12\text{ }\mu\text{m}$ ,  $10 - 14\text{ }\mu\text{m}$  and  $12 - 14\text{ }\mu\text{m}$ , respectively (Table S2).

Assuming this was due to the presence of peaks making the surface non-smooth, we wanted to get rid of them completely without creating holes. As we first wanted to know how much holes, as well as peaks, effect the result of segmentation, we projected both peaked (Figure 6A-B) and holed (Figure 6C-D) original tries. The result showed at least no visual distortion of the peaked projection (Figure 7A) while there were distortions in the holed projection.(Figure 7B). Focusing on the problem of holes we ran PaCeQuant on the projection (Figure 7C) and checked the distorted areas (Figure 7D-F). We observed introduced cut-offs (Figure 7E-F) and over-segmentation (Figure 7E). Even though it seemed as though the peaks had no big effect, we still decided to push for two workarounds for the smoothed-surface-objective while avoiding holes.

The first workaround used a Gaussian filter of 1  $\mu\text{m}$  as well as a high threshold of 5000 in order to remove peaks. As this introduced holes, we filled them by applying the *Fill Holes* function in MorphoGraphX three times. While this got rid of holes the valleys between two curved cells were also filled (Figure 7H). For the other workaround we applied a higher Gaussian filter of 3  $\mu\text{m}$  and used a low threshold of 1000 for edge detection. However, this placed the surface further from the actual one (Figure 7I). We applied the same method of checking errors as before to both workarounds. The distances for annihilation using the *fill-holes approach* for cotyledon 01 were chosen to be 8 – 10  $\mu\text{m}$  with  $e_{pc} = 3.60\%$ , 08 – 12  $\mu\text{m}$  with  $e_{pc} = 2.68\%$  and 10 – 12  $\mu\text{m}$  with  $e_{pc} = 0.93\%$  (Table S3). Applying these to all cotyledons resulted in a mean of 5.00% (SD=2.79%), 7.36% (SD=5.41%) and 7.83% (SD=5.58%) for 08 – 10  $\mu\text{m}$ , 08 – 12  $\mu\text{m}$  and 10 – 12  $\mu\text{m}$ , respectively (Table S4). For the high-Gaussian workaround the best annihilations were 10 – 14  $\mu\text{m}$  with  $e_{pc} = 1.77\%$ , 12 – 14  $\mu\text{m}$  with  $e_{pc} = 0\%$  and 10 – 16  $\mu\text{m}$  with  $e_{pc} = 1.80\%$  (Table S5). Resulting in a mean of 5.07% (SD=4.19%), 5.23% (SD=3.87%) and 6.43% (SD=3.82%) for 10 – 14  $\mu\text{m}$ , 12 – 14  $\mu\text{m}$  and 12 – 16  $\mu\text{m}$ , respectively (Table S6).

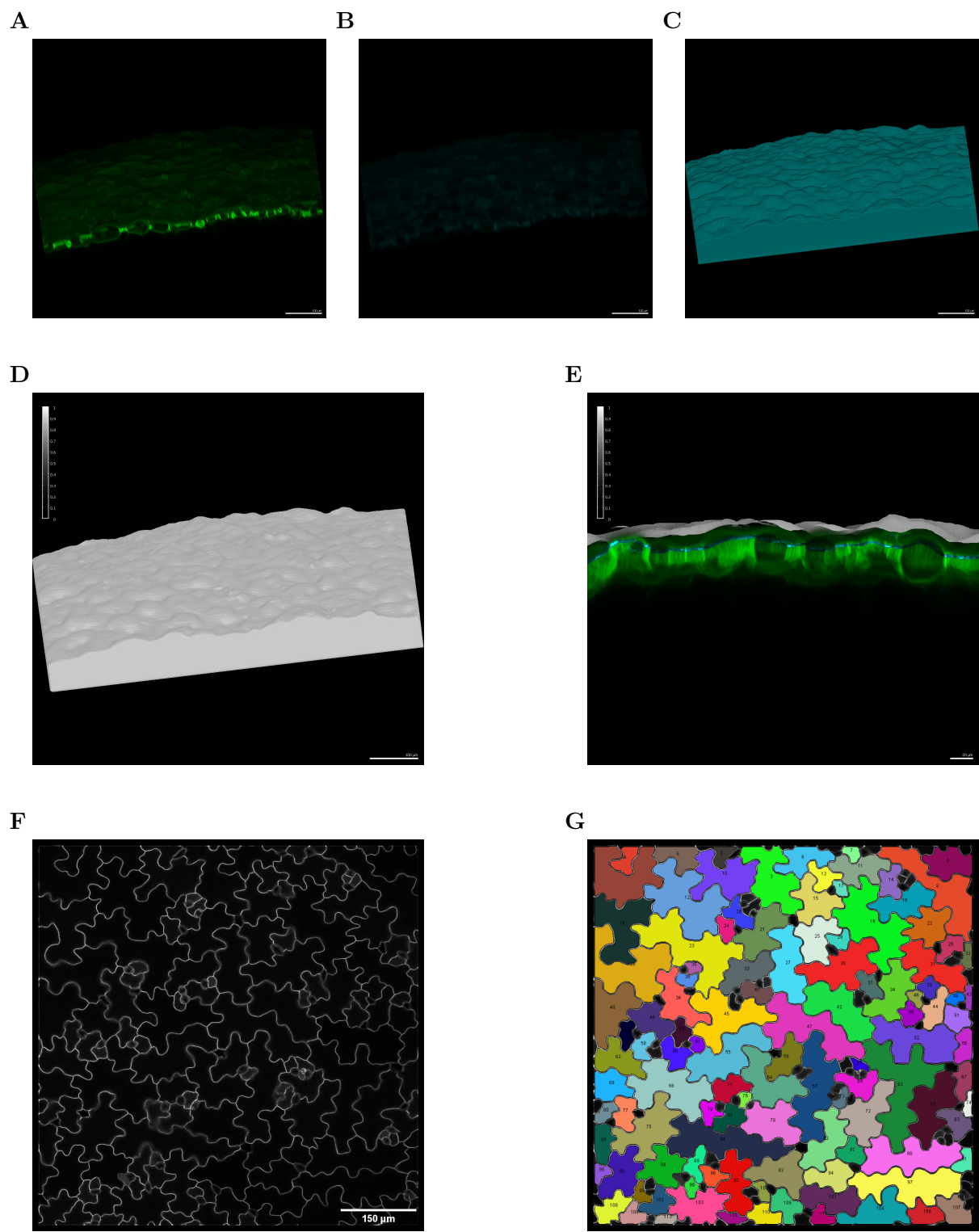


**Figure 5: MorphoGraphX general workflow.** (A) 3D depiction of cotyledon (01). (B) Gaussed stack ( $\text{Gauss} = 3$ ). (C) Detected Edge (T1000). (D) Extracted Surface ( $5 \mu\text{m}$  cube size). (E) Main, un-Gaussed stack (green), extracted surface (white) and stack after annihilation (blue). (F) MAX-z-projection after trimming the bottom. (G) Colored PaCeQuant segmentation result of the MAX-z-projection. Scale bars: (A-D):  $100 \mu\text{m}$ ; (E):  $20 \mu\text{m}$ .

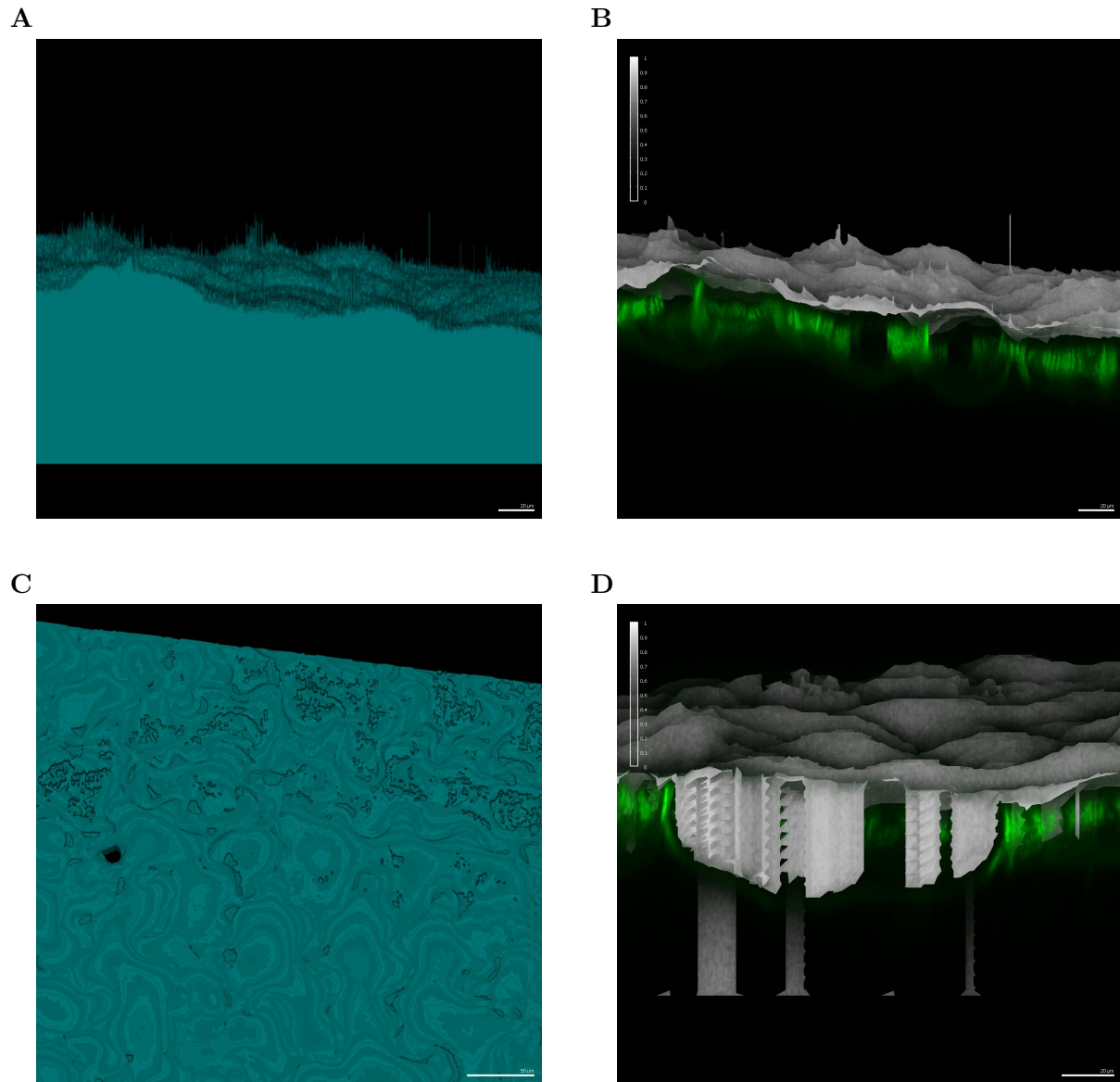


**Figure 6: The edge detect threshold dilemma.** (A-B) Cotyledon (01) processed with a Gaussian of 0.3 and a edge detect threshold of 2000. Edge and Surface with main stack, respectively. (C-D) Cotyledon (01) processed with a Gaussian of 1 and an edge detect threshold of 5000. Edge and Surface with main stack, respectively. Scale bars: (A-B,D): 20  $\mu\text{m}$ ; (C): 50  $\mu\text{m}$ .

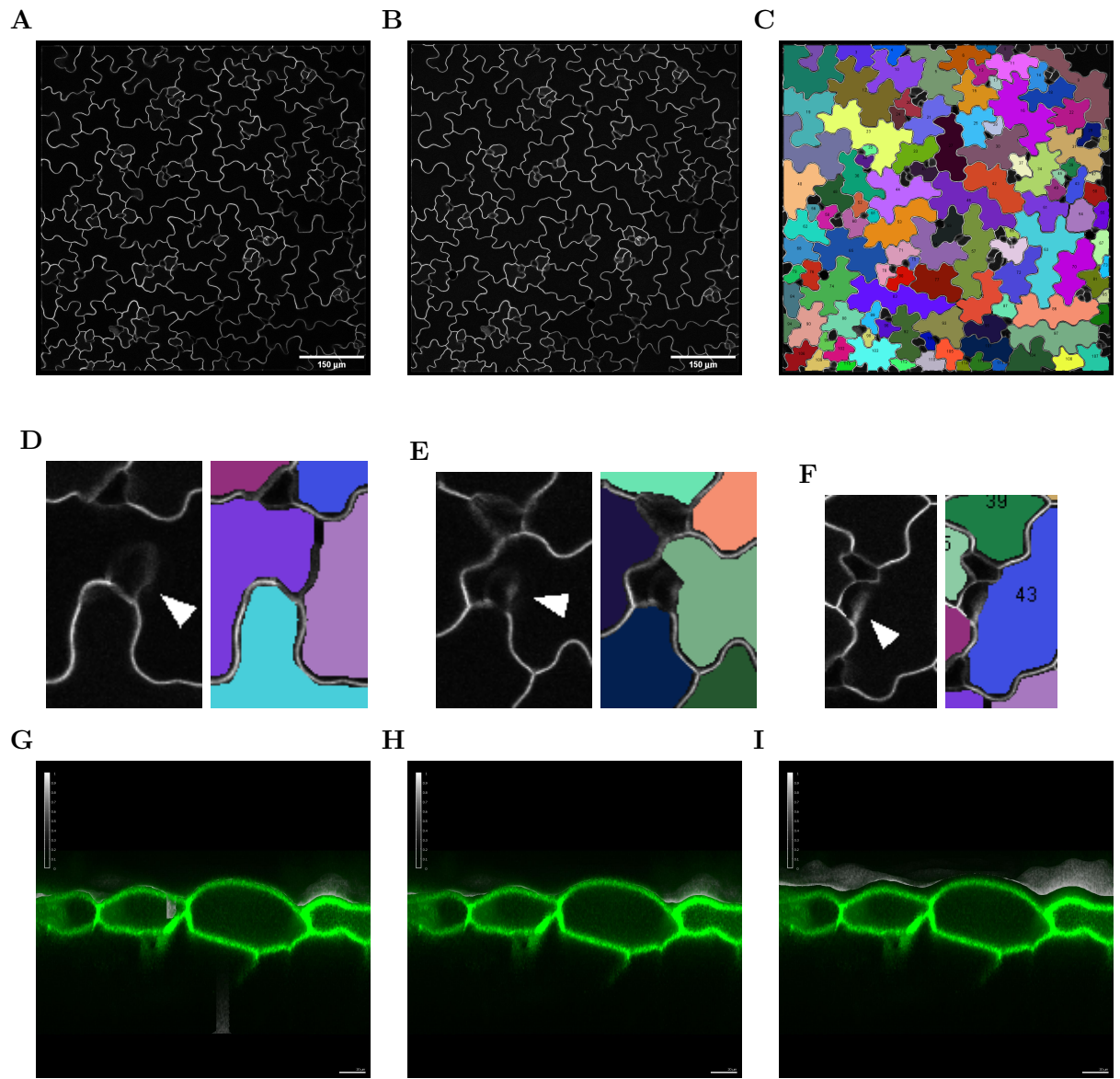


**Figure 7: Problem of holes in the surface and two additional ways to fix it.** (A) projection of g0.3T2000 ("peaks"). (B) projection of g1T5000 ("holes"). (C) Colored PaCeQuant segmentation result of g1T5000. (D-F) Projection of g1T5000 on the left (white arrow tips show region of interest), segmentation on the right. Holes affect the segmentation. (G) Clip of g1T5000. (H) Clip of g1T5000 after having applied fill-holes function three times before surface extraction. This got rid of the holes but introduced artifacts between two cells at the surface. (I) Clip of g3T5000. A higher Gaussian results in no holes, but a more loosely associated surface. Scale bars: (G-I): 20  $\mu\text{m}$ .

## 2.3 Epifluorescent Widefield- or Confocal Microscopy

To convince ourselves which imaging technique to capitalize, we have imaged 7 day old cotyledons using various objective lenses for widefield epifluorescent- as well as confocal-microscopy. For all objective lenses the former gave high resolution images (Figure 8ACE) whereas widefield epifluorescence microscopy yielded noisy results (Figure 8BDF). This was repeated for cleared tissue with similar results, but better results for the 60x oil-immersed widefield objective (Figure S4). To figure out whether the fast epifluorescent widefield images could be used for our workflow we analyzed the stacks of the 60x oil-immersion objectives using MorphoGraphX (Figure 9A-D). The stack for both the fresh and clear tissue were loaded (Figure 9A and Figure 9C, respectively). Afterwards, we applied a Gaussian filter of  $2\text{ }\mu\text{m}$  and detected the edges (Figure 9B and Figure 9D, respectively), which marks the step before surface extraction. The stacks themselves show a great amount of noise which is apparent as the surface was not visible. This was reflected in the result of edge detection which yielded the surface for some cells and did not detect it for others, leaving gauged out cells. Multiple values were tested, with the values used here being the best ones deemed by us. Going higher with the Gaussian filter was possible at the cost of processing time. Using a Gaussian filter of  $3\text{ }\mu\text{m}$  did not improve the result per eye and using a Gaussian filter of  $5\text{ }\mu\text{m}$  exceeded the memory capacity of the machine used for processing (16 GB).

To further show the problem we analyzed the surface of one cell of a widefield 20x stack of the analyzed cotyledon (Figure 9E-G) using Fiji. When resolution is enough, we observed the cell borders closing into the cell while going through the stack to the top. This depicts the surface. However, using widefield microscopy this border melted with the noise and was not visible in certain areas (Figure 9E-F). In this case, we chose one image of the stack where the top cell border was partially visible (Figure 9E-F, red arrows). However, this border was not complete, and did also not appear when going through the stack. Thus, the surface border was melted with the noise. To quantify this we analyzed the intensity going through where the border ought to close using the *plot profile* task in Fiji (Figure 9G). One could image the cell border to be in the middle where it is expected and the signal to be highest there. However, the difference between this and the noise was hardly visible. We believe that this explains the problems with the edge detection using MorphoGraphX. At the very least, this shows that widefield images are noisy.

Lastly, using a 10x dry objective at a confocal microscope we wanted to see whether the resolution was enough. While the xy resolution may have been enough Figure 9H the z resolution was not enough as the resulting z-step size was too high (not shown).

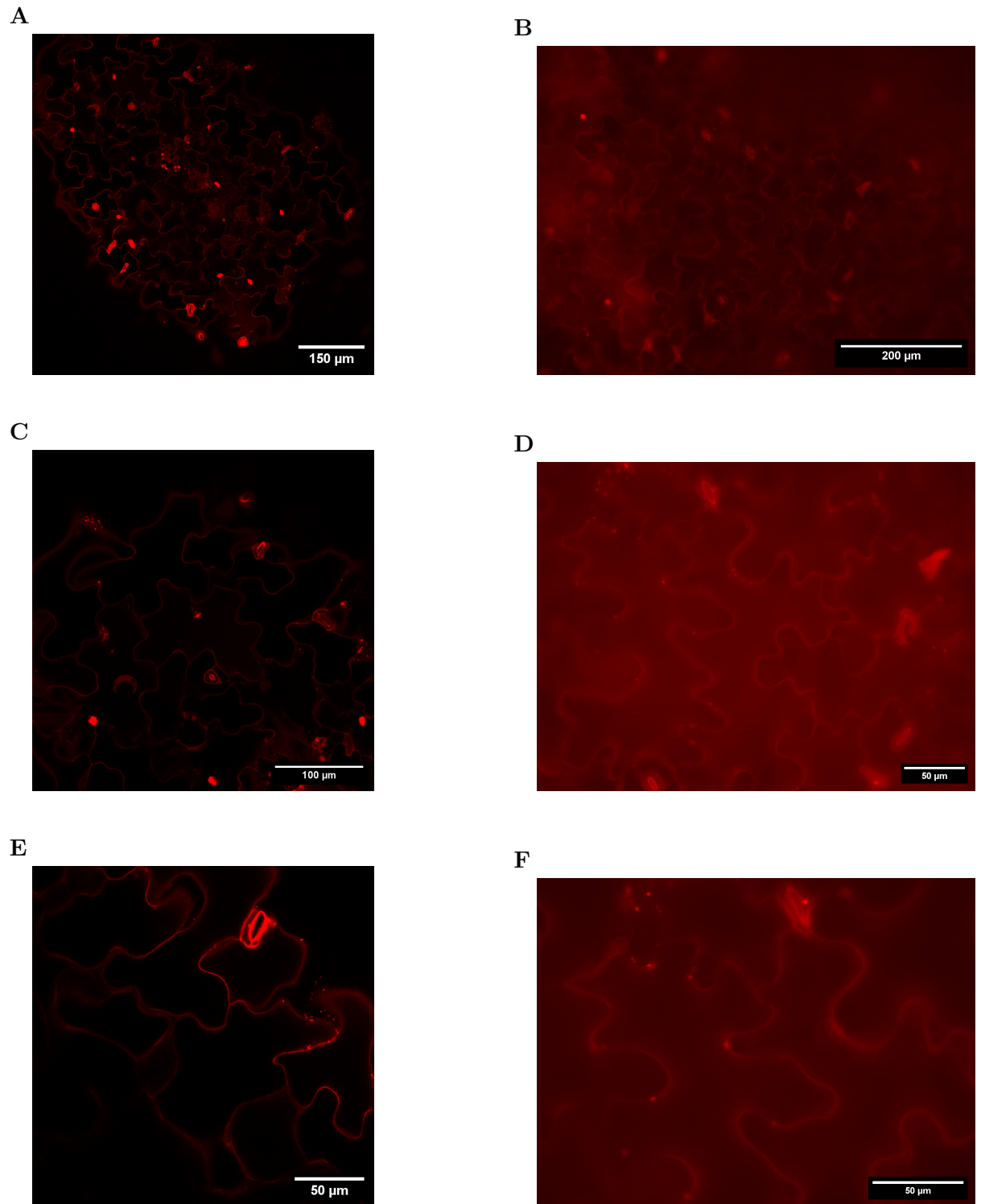


**Figure 8: Widiefield vs Confocal Propidium Iodide.** All Images were taken from the same cotyledon. (A,C,E) Confocal microscopy: (A) 20x-w-cf, (A) 40x-w-cf, (A) 63x-w-cf. (B,D,F) Widefield microscopy: (B) 20x-dry-wf, (D) 40x-dry-wf, (F) 60x-oil-wf.

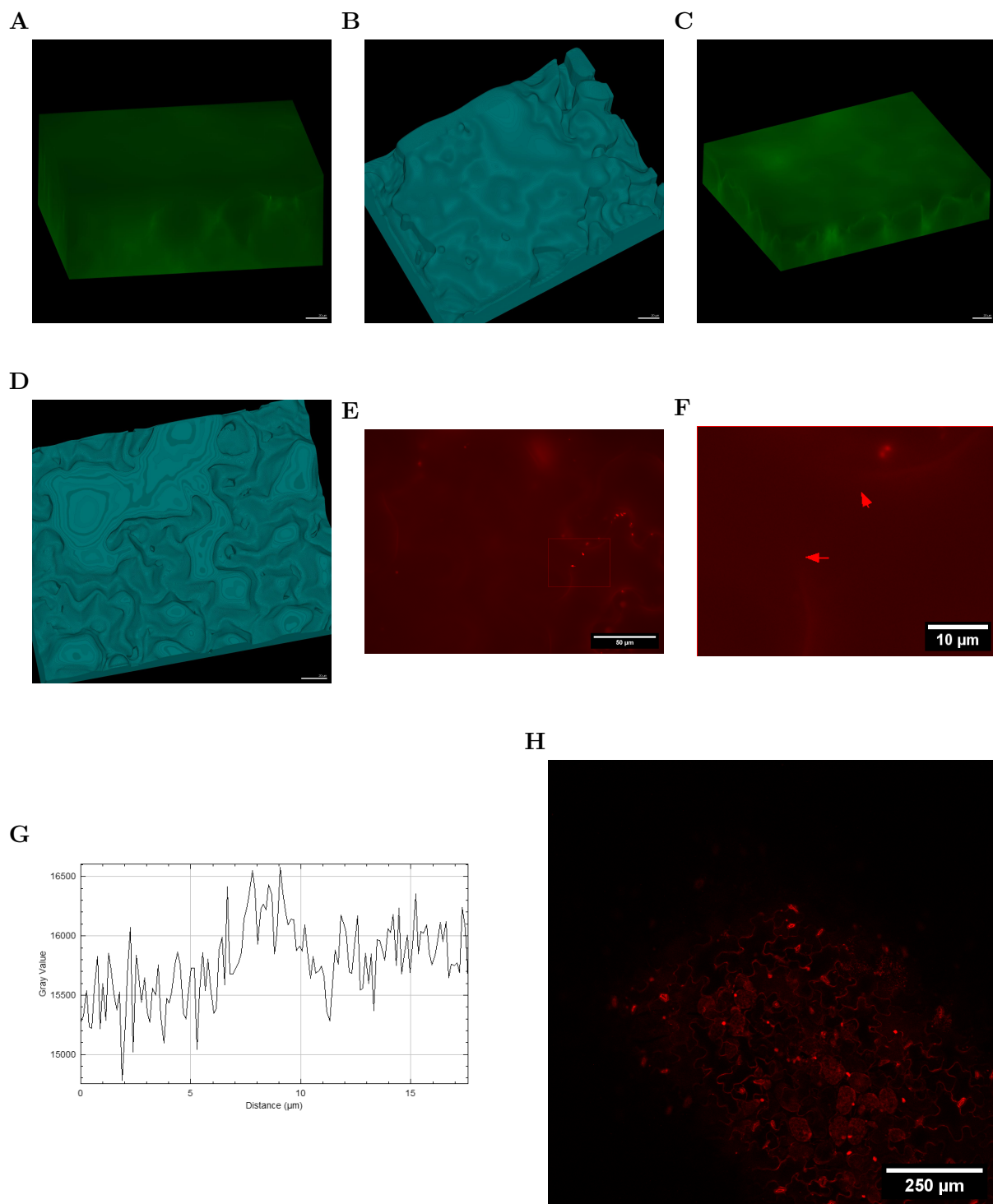


**Figure 9: Investigation of noise level and workflow compatibility.** (A) 3D depiction of fresh PI-stained tissue; 60x-oil-wf. (B) edge detect of (A) with Gauss1,  $T=15000$ . (C) 3D depiction of fixed and cleared calcofluor white stained tissue; 60x-oil-wf. (D) edge detect of (C) with Gauss1,  $T=22000$ . (E) Surface border of fresh PI-stained tissue, (F) cropped out from (E): two red arrows indicate the surface border. (G) Signal plotted between arrows perpendicular through where the surface border ought to have been. (H) fresh PI-stained tissue; 10x-dry-cf. Scale bars: (A-D): 20  $\mu\text{m}$ .

## 2.4 Decreasing Preparation Time

When using fresh tissue it is important that preparation as well as imaging time is as little as possible as this may create a bias when comparing genotypes or growth conditions. We tried using stained media using propidium iodide (PI) (Figure 10) or Calcofluor White (Figure 11) in various concentrations 6dag.

In the case of PI we tested concentrations ranging from  $0.1 \frac{\mu\text{g}}{\text{mL}}$  to  $100 \frac{\mu\text{g}}{\text{mL}}$  (Figure 10). To show low-intensity images, all images were altered using *enhance contrast* of 0.35 with normalization on in Fiji. Compared to a freshly  $0.2 \frac{\mu\text{g}}{\text{mL}}$  PI-stained plant (Figure 10A),  $0.1 \frac{\mu\text{g}}{\text{mL}}$  and  $1 \frac{\mu\text{g}}{\text{mL}}$  PI-stained media resulted in blurry cell borders and a weak signal (Figure 10B-C). In contrast,  $10 \frac{\mu\text{g}}{\text{mL}}$  and  $100 \frac{\mu\text{g}}{\text{mL}}$  (Figure 10D-F) resembled the intensity of freshly stained tissue. However, using these high concentrations in the media also resulted in the inside of the cell being stained significantly. Further, using  $100 \frac{\mu\text{g}}{\text{mL}}$  PI in the media stunted the growth of the plants (Figure 10F). To summarize, a concentration between  $10 \frac{\mu\text{g}}{\text{mL}}$  and  $100 \frac{\mu\text{g}}{\text{mL}}$  worked best.

We tested Calcofluor White pre-stained media for concentrations ranging from  $1.4 \frac{\mu\text{g}}{\text{mL}}$  to  $1400 \frac{\mu\text{g}}{\text{mL}}$  (Figure 11) with the idea and the original order of concentration,  $1.4 \frac{\mu\text{g}}{\text{mL}}$ , being taken from a paper ([BIDHENDI et al. 2020](#)). To show low-intensity images, all images were altered using *enhance contrast* of 0.35 with normalization on with Fiji. In all cases we observed weak cell-border signals. For all images we observed bright spots in comparison to the cell border signal. For  $1.4 \frac{\mu\text{g}}{\text{mL}}$  and  $14 \frac{\mu\text{g}}{\text{mL}}$  these bright spots were stomata (Figure 11A-B), whereas for the highest concentrations they were seemingly at random positions (Figure 11C-D). By eye the plants did not show any changes in growth (not shown).  $14 \frac{\mu\text{g}}{\text{mL}}$  had a seemingly better signal to noise than  $1.4 \frac{\mu\text{g}}{\text{mL}}$  and did not show any randomly distributed bright dots (Figure 11B).

As already described, we also made use of an *Arabidopsis* line expressing mCherry specifically in the plasma membrane of epidermal tissue, thus marking only the PCs. Following on the idea of decreasing time by using already-stained plants we tried an in-growth-plate imaging approach with a 25x water dipping objective. Using this, the dish containing the plants could simply be covered with water and directly imaged without the need of preparing the plants on a slide. As they are free to move in this approach we sought to investigate whether they moved and if they did whether it would disturb the imaging process. For this, we used the mCherry expressing line 6dag, marked three plants, filled the dish with water and imaged using the 25x dipping objective. Afterwards, these cotyledons were imaged using the 20x water immersion objective. Imaging was performed for five minutes while taking an image each 10 s. Using Fiji we changed the color of the first image to magenta and of the last to green using the lookup-tables. Then, the images were merged using the respective function in Fiji. The non-dipping method results in a slight change in z-direction in the five minutes (Figure 12ACE). In contrast, the dipping method shows a significant change in all three cases (Figure 12BDF). There was not only a z-shift but also a xy-shift.

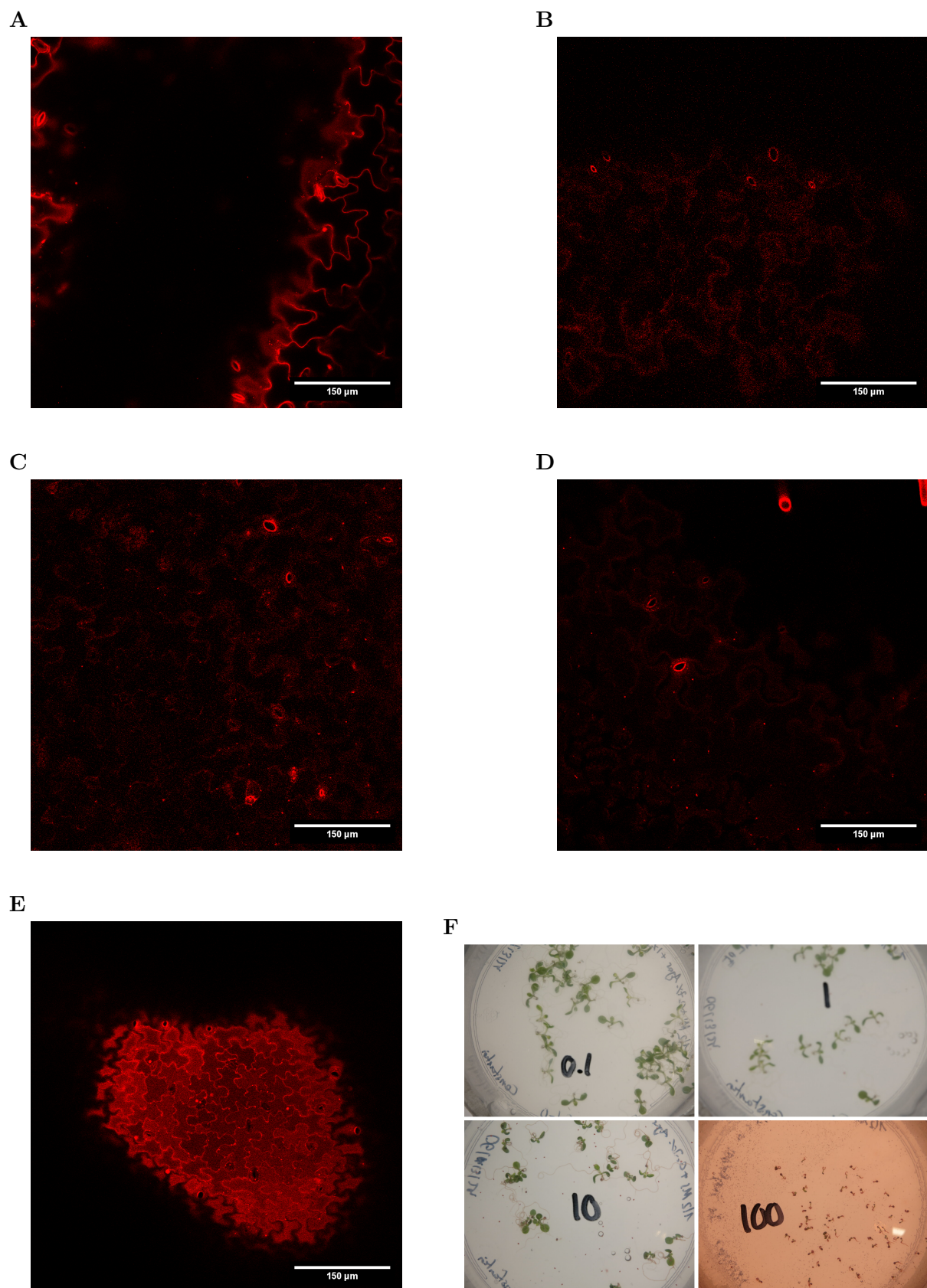


**Figure 10: PI pre-stained medium.** Confocal images of PI growth-stained cotyledons were contrast enhanced with a value of 0.35, normalized, using Fiji. (A) Control, Freshly PI-stained Cotyledon. (B-E) PI-plates: (B)  $0.1 \frac{\mu\text{g}}{\text{mL}}$ , (C)  $1 \frac{\mu\text{g}}{\text{mL}}$ , (D)  $10 \frac{\mu\text{g}}{\text{mL}}$ , (E)  $100 \frac{\mu\text{g}}{\text{mL}}$ ; 20x-w-cf (F) Plates in which the analyzed plants grew in.

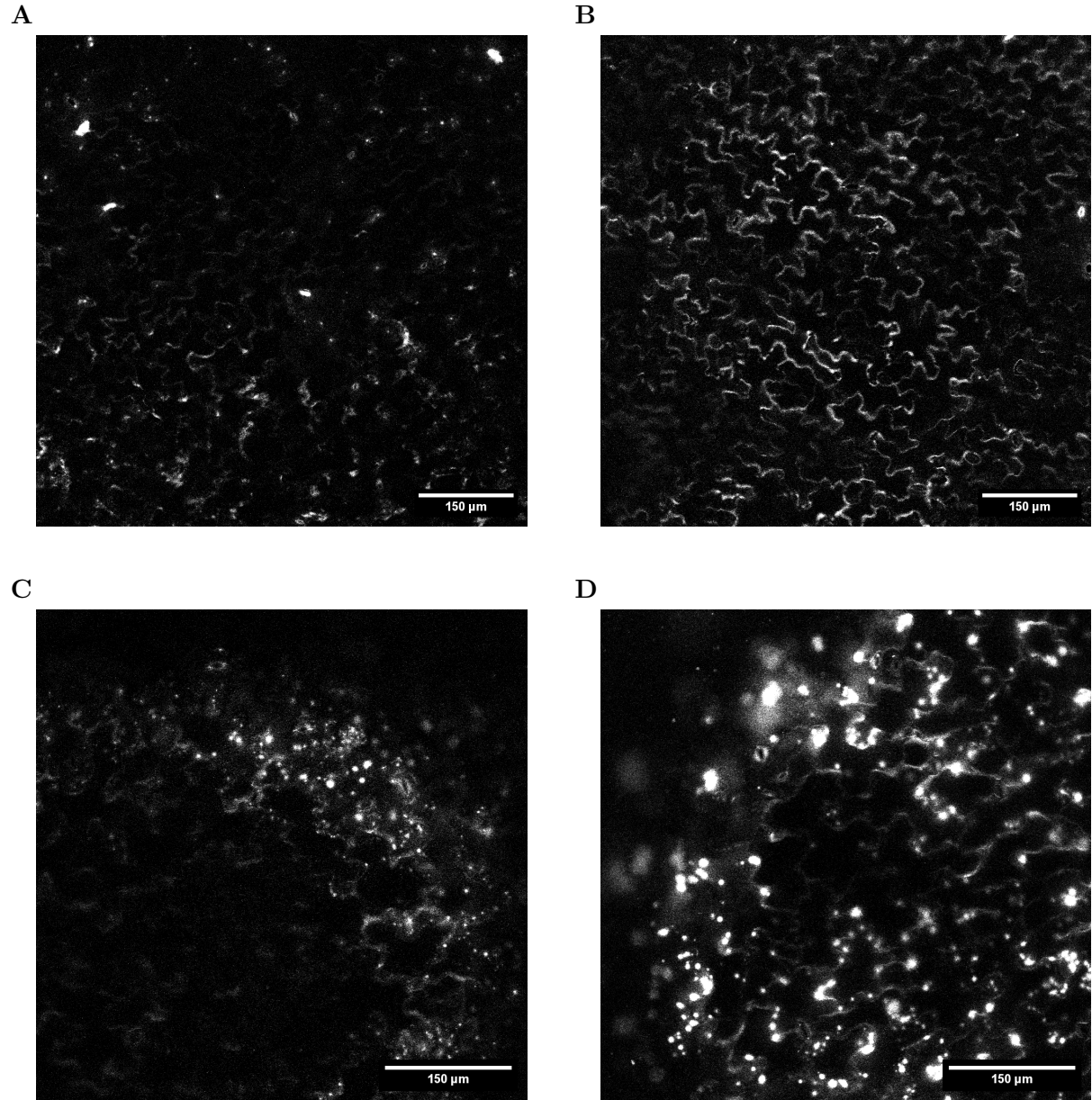


**Figure 11: Calcofluor white pre-stained medium.** Confocal images of calcofluor white growth-stained cotyledons were contrast enhanced with a value of 0.35, normalized, using Fiji. (A)  $1.4 \frac{\mu\text{g}}{\text{mL}}$  (B)  $14 \frac{\mu\text{g}}{\text{mL}}$ , (C)  $140 \frac{\mu\text{g}}{\text{mL}}$ , (D)  $1400 \frac{\mu\text{g}}{\text{mL}}$ ; 20x-w-cf

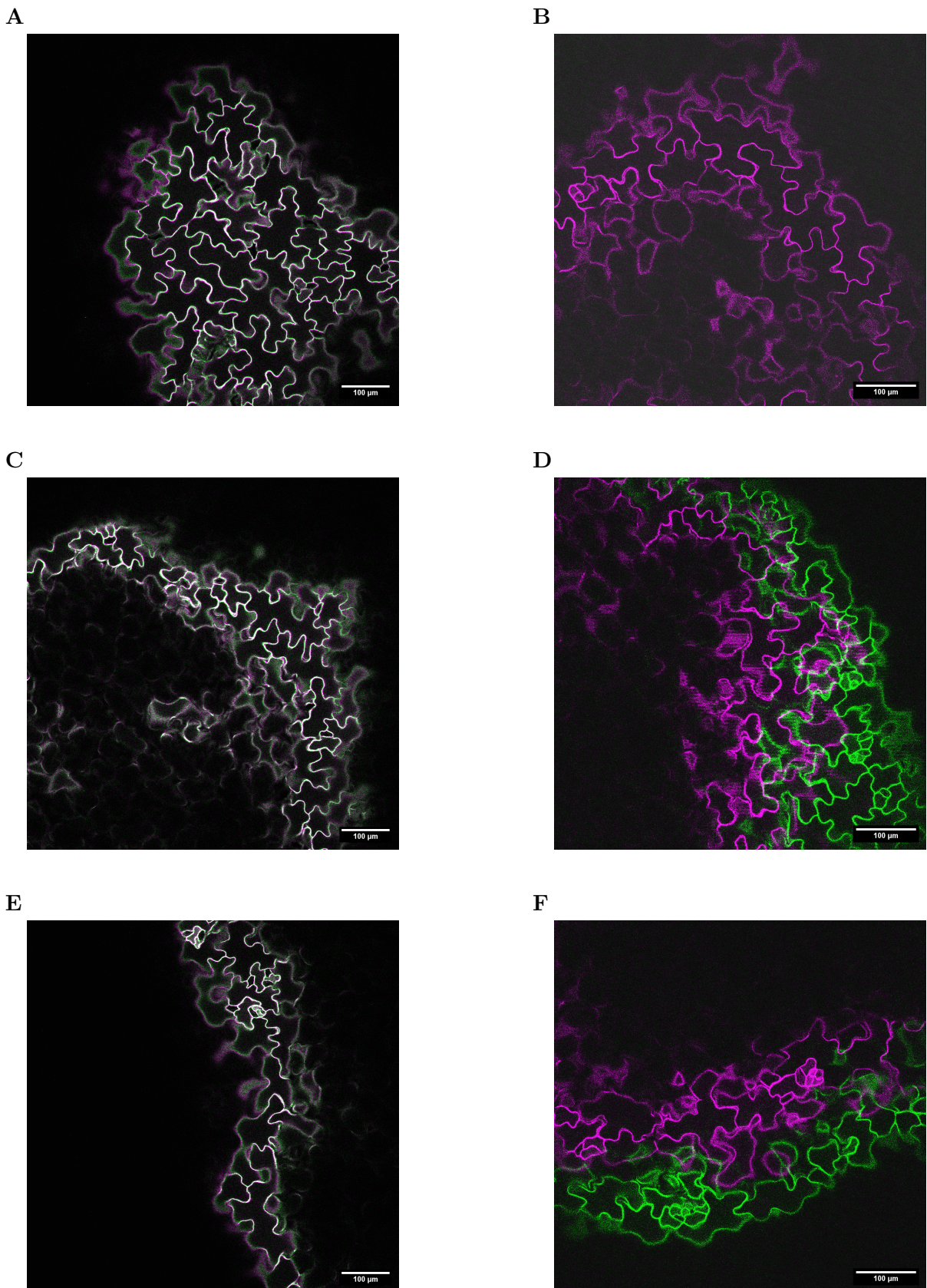


**Figure 12: Time Analysis of mCherry line using a dipping and immersion objective.** The same cotyledon was imaged with both the 25x-dip-cf and 10x-w-cf. Each time a time serie of 5 minutes was created. Using Fiji, the starting image was turned magenta and the image after the five minutes was turned green (using LUTs), afterwhich the were merged using Fiji. (A,C,E): cotyledons imaged using the normal strategy, i.e. water-immersion objective. (B,D,F): cotyledons imaged using a dipping objective.

### 3 Discussion

Here we have tried to adapt an already established workflow for quantifying the shape of pavement cells. We have presented our issues from fixed and cleared tissue to cell segmentation errors.

#### 3.1 Fixed and Cleared Tissue Does Not Conserve the Native Cell Structure

By comparing Col-0 cotyledons of fresh tissue to fixed and cleared tissue we have shown the non-native state of the cell surface in the latter case. Further, we have shown that this is not due to an excessive amount of time in the clearing solution as it also appears 1 month and 10 days after fixation. Given our findings we hypothesize that this is due to the initial clearing process. This could be tested by observing the tissue directly after clearing the cotyledons, i.e. a few days after fixation. Our main reason for using fixed and cleared tissue is to be flexible in experimental design as fixation halts tissue growth. Because of this, even if the tissue would still be native after a few days it would not provide the qualities we are looking for. However, it is not safe to assume that fixation and clearing both lead to the non-native cell shape. While it could very well be the case that this is simply due to a prolonged time in any aqueous solvent, the clearing agent ClearSee could also be responsible. Thus, it would be of interest to image fresh tissue after it has been in water for some time as well as test whether just fixing the tissue will have the same effect of fixing and clearing. Further, the fixation protocol ([Ursache et al. 2018](#)) suggests to use no vacuum for 5-and 6-day old *Arabidopsis* seedlings. As we fixed seven day old tissue, we opted to use a vacuum. Fixation ought to be repeated with no vacuum.

Regardless, while we decided against fixed and cleared tissue at an early point of work, seeing how the other approaches have their own issues we may be inclined to test the workflow of surface extraction on fixed and cleared tissue further.

Another observation was that fresh tissue can also be flattened by simply laying it on the inverted chamber-slide (Figure 1A, Figure 2C). Despite this observation for this one fresh cotyledon, we have not observed such a thing in any of the other dozens of fresh cotyledons beforehand. It may very well be the case that we accidentally pressed it with the forceps against the slide. To test this, we ought to repeat this experiment.

#### 3.2 Using MorphoGraphX to Overcome Cell and Tissue Curvature

Having decided upon using fresh tissue over cleared tissue, we faced the issue of curved cell and tissue surface of pavement cells in cotyledons. We showed that a simple maximum projection, or it being coupled with rolling background subtraction with pixel size one, yields too many errors (about 40% per (corrected) cell). Also, it is important to remember that we used an *Arabidopsis* line expressing mCherry specifically localized in the plasma membrane of epidermal tissue, thus marking only the pavement cells and stomata-associated cell in the cotyledon. We believe that the weak signal found under the epidermal layer is due to the autofluorescence of the plant tissue. Thus, we have reason to believe that such an approach would turn out even worse for stained tissue. The projections, using no MorphoGraphX, have also been made for the other five cotyledons. However, since by eye they appeared equally as flawed, the error rate being so high and keeping accurate track of so many errors is difficult, we have decided not to invest the

time into it and assume it as a non-working model.

Using MorphoGraphX we were able to show a better workflow. We established that ideally the surface is smooth with no holes and tightly fit around the surface signal. However, achieving the first two at the same time proved difficult for low Gaussian filter values. Further we showed that holes in the surface, resulting from a too high edge detect threshold  $T$ , affects the segmentation. Thus, we produced three workflows that would either avoid creating holes or fix them afterwards. First, by allowing a slight non-smooth surface by decreasing  $T$  avoided holes (G1T1000). Second, deliberately choosing a high threshold to create **small** holes (as large ones can hardly be closed using this method) which are filled afterwards by applying the standard fill-holes function in MorphoGraphX. And third, applying a high Gaussian filter allowed us to use a low  $T$  while not getting an unsmooth surface. However, seemingly all approaches have their flaws: The first will yield a non-smooth surface. The second yielded filled cell-valleys. And the third leaded to a loose surface attachment. We then tested the robustness of each workflow by applying PaCeQuant to the resulting projections. The results are summarized in Table 5. In regards to the lowest means and lowest standard deviation, on average the Gaussian workflow is the best, with fill-holes second and G1T1000 last. However, in regards to the best singular projection, the fill-holes workflow is the best with 5.00% (SD=2.79%) being the lowest mean, and the lowest standard deviation by far. As this is no statistical test, and they are quite close to each other we can not make any statement about whether they differ or not. However, the amount of errors is still too high to work with any of the workflows which pushes us to rather try something different than lament of which of these is slightly better.

**Table 5:** Mean and standard deviation of errors per (corrected) cells  $e_{pc}$  for each workflow to combat the hole-problem. The values for all three annihilations are shown. Note that these are not ordered.

|            | $e_{pc}(\text{annih1})$ | $e_{pc}(\text{annih2})$ | $e_{pc}(\text{annih3})$ |
|------------|-------------------------|-------------------------|-------------------------|
| G1T1000    | 6.80% (SD=4.68%)        | 6.99% (SD=5.10%)        | 7.84% (SD=4.55%)        |
| Fill-Holes | 5.00% (SD=2.79%)        | 7.36% (SD=5.41%)        | 7.83% (SD=5.58%)        |
| Gaussian   | 5.07% (SD=4.19%)        | 5.23% (SD=3.87%)        | 6.43% (SD=3.82%)        |

One reason could be a too low signal to noise ratio. We could test this by scanning the same stack once without any line averaging, as was done here, and once with a high amount of line averaging.

Alternatively, we could also try to do the segmentation directly in MorphoGraphX. This would have the disadvantage of losing the many PC-related parameters which are easily accessible with PaCeQuant. However, another argument could be made for MorphoGraphX. By projecting the stack into 2D all curvature in the segmentation any parameters, e.g. cell area, are falsified with a varying decree depending on the curvature. Since we have observed quite curved tissue among these six tested cotyledons, it would be right to assume that this problem may arise in the future.

Further, we would like to go back and screen for g0.3T1000 (Figure 6A, Figure 6B). Initially we believed the peaks to be as destructive of the segmentation as holes are. But, we should try it rather than assume it.

### 3.3 Epifluorescent Microscopy Images are Noisy

We verified that using epifluorescent microscopy proofs difficult for our workflow as the noise is not separable with the cell surface for freshly stained tissue with PI (Figure 9). Interestingly, the signal to noise ratio appear to be better for fixed and cleared tissue Figure S4. As the quality of the image often directly affects the segmentation, many decide to use confocal microscopy. Compared to, for example, widefield epifluorescent microscopy the addition of a pinhole in the confocal microscope allows the capture of a single plane at the time. The result is an increase in depth-resolution, just as we have observed. However, besides the apparent advantage the confocal microscopy has major drawbacks. Time and money. Frankly, many labs do not have a confocal microscope, especially in poorer countries like Spain. In the case of an institute owning a confocal microscopy there is still a problem with time as often one or a few machines are used by the entire faculty. In order to avoid the use of confocal microscopy one could employ a deep-learned model which could denoise widefield images. One such deeplearning tool would be content-aware image restoration ([Weigert et al. 2018](#)). Many pre-trained models already exist, are free to use and can be, for example, found at BioImage.io. We encourage interested scientists to look for already pre-trained models as it can save valuable time. Do however note these denoising deep-learned models are highly task-specific. Thus, one should not expect to make use of a model trained for a different type of tissue without a valid reason to do so.

### 3.4 There Is (Currently) No Free Lunch

Besides image quality, capture speed is another deciding factor. For example, imaging can be performed without line averaging, as we have done here, or using lower dwell times by increasing the scan frequency, which does come at the cost of area as one has to zoom in. Scan time can be brought to the max by using a resonant scanner which increases scan time significantly at the cost of noise. Again, using line averaging this noise can be combated at the cost of speed. Further, one can also deploy bidirectional scanning, something we also have not done here yet. For us this trade-off will be very important as we decided, at least for now, to use fresh tissue. We may need more picture quality, e.g. through higher line averaging, but this would come at the cost of speed. As we are working with live tissue, it will change while we scan others. Thus, keeping scan, as well as preparation time, as low as possible is also key.

Here we mainly tried to decrease tissue preparation time by using pre-stained media or a line already marking the PCs with mCherry. This would make a dye-incubation step obsolete. In this regard we showed that the mCherry expressing line worked well, while the stained-media plates worked rather poorly. While there are some candidates among the stained media plates that have a signal but do not show any bright dots, likely sequestered dye, or staining of the cytoplasm, their signal is weak and the noise is comparatively high. Further, PI clearly has a stunting growth effect on seedlings when used in excess.

The mCherry line may be working well but it does also have a major drawback. Namely, if we want to apply this method to genotypes, which is something we want to do, we would need to cross each genotype with this marker line which may not be worth the trouble.

In addition to this, we wanted to reduce the preparation time, e.g. of the mCherry line, further by scanning in the plate the plants grew in. This is possible by flooding the plate with

distilled water and using a water-dipping microscope. However, we found there to me significant movement, likely both in z-direction as well as the xy-plane.

## References

- BIDHENDI, A.J. et al. (2020). “Fluorescence visualization of cellulose and pectin in the primary plant cell wall”. In: *Journal of Microscopy* 278.3, pp. 164–181. DOI: <https://doi.org/10.1111/jmi.12895>. eprint: <https://onlinelibrary.wiley.com/doi/pdf/10.1111/jmi.12895>. URL: <https://onlinelibrary.wiley.com/doi/abs/10.1111/jmi.12895>.
- Erguvan, Özer et al. (May 2019). “ImageJ SurfCut: a user-friendly pipeline for high-throughput extraction of cell contours from 3D image stacks”. In: *BMC Biology* 17.1. ISSN: 1741-7007. DOI: 10.1186/s12915-019-0657-1. URL: <http://dx.doi.org/10.1186/s12915-019-0657-1>.
- Möller, Birgit et al. (Sept. 2017). “PaCeQuant: A Tool for High-Throughput Quantification of Pavement Cell Shape Characteristics”. In: *Plant Physiology* 175.3, pp. 998–1017. ISSN: 0032-0889. DOI: 10.1104/pp.17.00961. eprint: [https://academic.oup.com/plphys/article-pdf/175/3/998/37245904/plphys\\_v175\\_3\\_998.pdf](https://academic.oup.com/plphys/article-pdf/175/3/998/37245904/plphys_v175_3_998.pdf). URL: <https://doi.org/10.1104/pp.17.00961>.
- Schindelin, Johannes et al. (June 2012). “Fiji: an open-source platform for biological-image analysis”. In: *Nature Methods* 9.7, pp. 676–682. ISSN: 1548-7105. DOI: 10.1038/nmeth.2019. URL: <http://dx.doi.org/10.1038/nmeth.2019>.
- Smit, Margot E. et al. (2023). “Extensive embryonic patterning without cellular differentiation primes the plant epidermis for efficient post-embryonic stomatal activities”. In: *Developmental Cell* 58.6, 506–521.e5. ISSN: 1534-5807. DOI: <https://doi.org/10.1016/j.devcel.2023.02.014>. URL: <https://www.sciencedirect.com/science/article/pii/S1534580723000734>.
- Strauss, Soeren et al. (2021). “MorphoGraphX 2.0: Providing context for biological image analysis with positional information”. In: *bioRxiv*. DOI: 10.1101/2021.08.12.456042. eprint: <https://www.biorxiv.org/content/early/2021/08/13/2021.08.12.456042.full.pdf>. URL: <https://www.biorxiv.org/content/early/2021/08/13/2021.08.12.456042>.
- Ursache, Robertas et al. (2018). “A protocol for combining fluorescent proteins with histological stains for diverse cell wall components”. In: *The Plant Journal* 93.2, pp. 399–412. DOI: <https://doi.org/10.1111/tpj.13784>. eprint: <https://onlinelibrary.wiley.com/doi/pdf/10.1111/tpj.13784>. URL: <https://onlinelibrary.wiley.com/doi/abs/10.1111/tpj.13784>.
- Weigert, Martin et al. (Nov. 2018). “Content-aware image restoration: pushing the limits of fluorescence microscopy”. In: *Nature Methods* 15.12, pp. 1090–1097. ISSN: 1548-7105. DOI: 10.1038/s41592-018-0216-7. URL: <http://dx.doi.org/10.1038/s41592-018-0216-7>.

## Supplementary

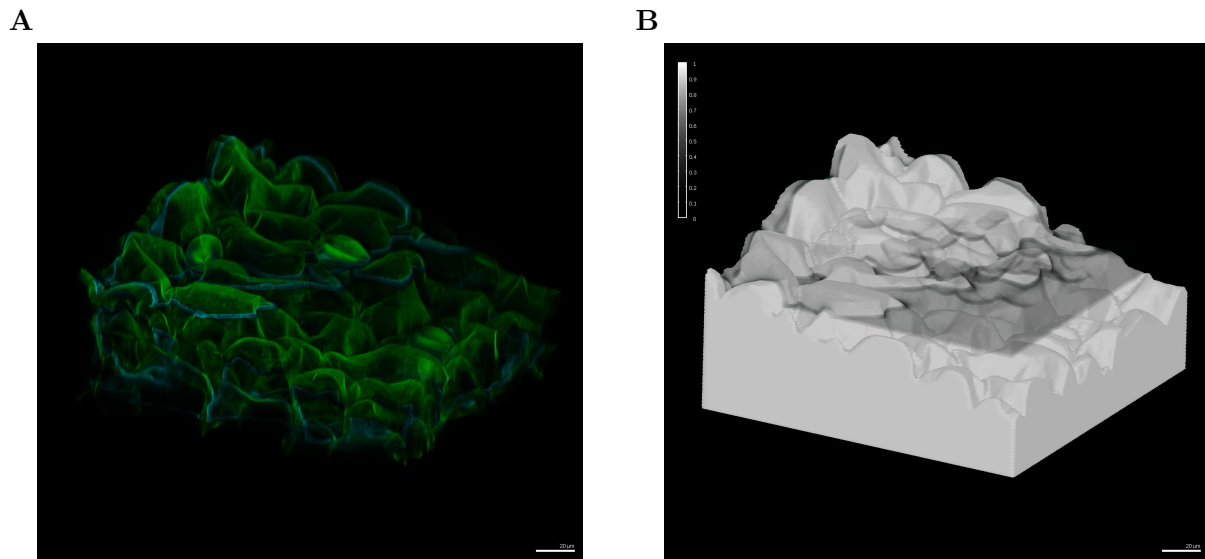


**Figure S1: Attempt to follow MorphoGraphX workflow with fixed and cleared (nothing).** (A) Cotyledon with nothing on top it's back from Figure 1B. Main stack (green) as well as remaining stack after annihilation (blue) are shown. (B) Cotyledon with nothing on top it's back from Figure 1B. Surface (white) as well as remaining stack after annihilation (grey) are shown. Scale bars: 20 μm.

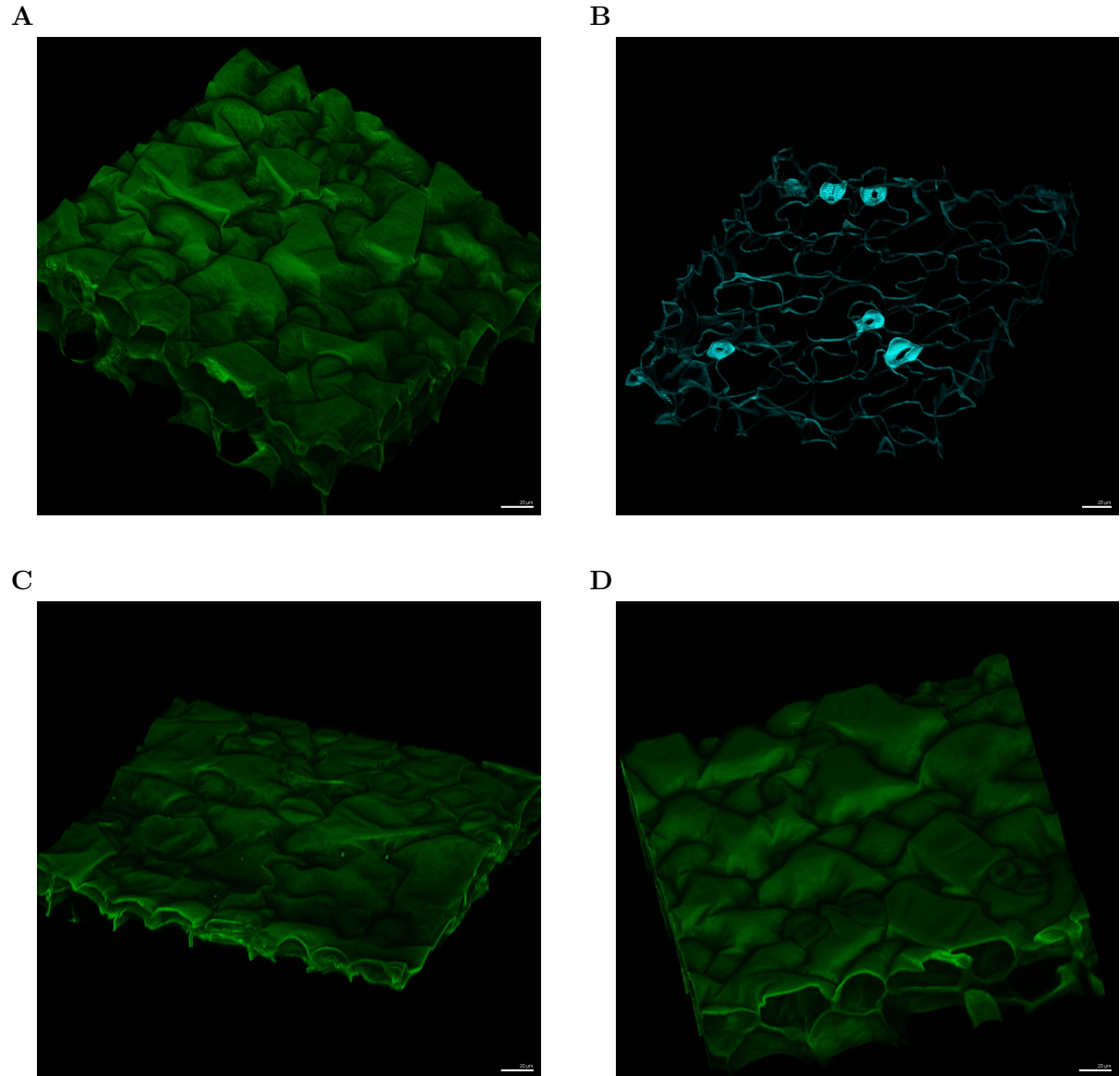


**Figure S2: Repeat of Figure 1, one month in ClearSee.** (A) Cotyledon with nothing on top and (B) successful remaining stack after annihilation (blue) is shown. (C) Cotyledon with slide on top. (D) Cotyledon with agar on top. Scale bars: 20  $\mu$ m.

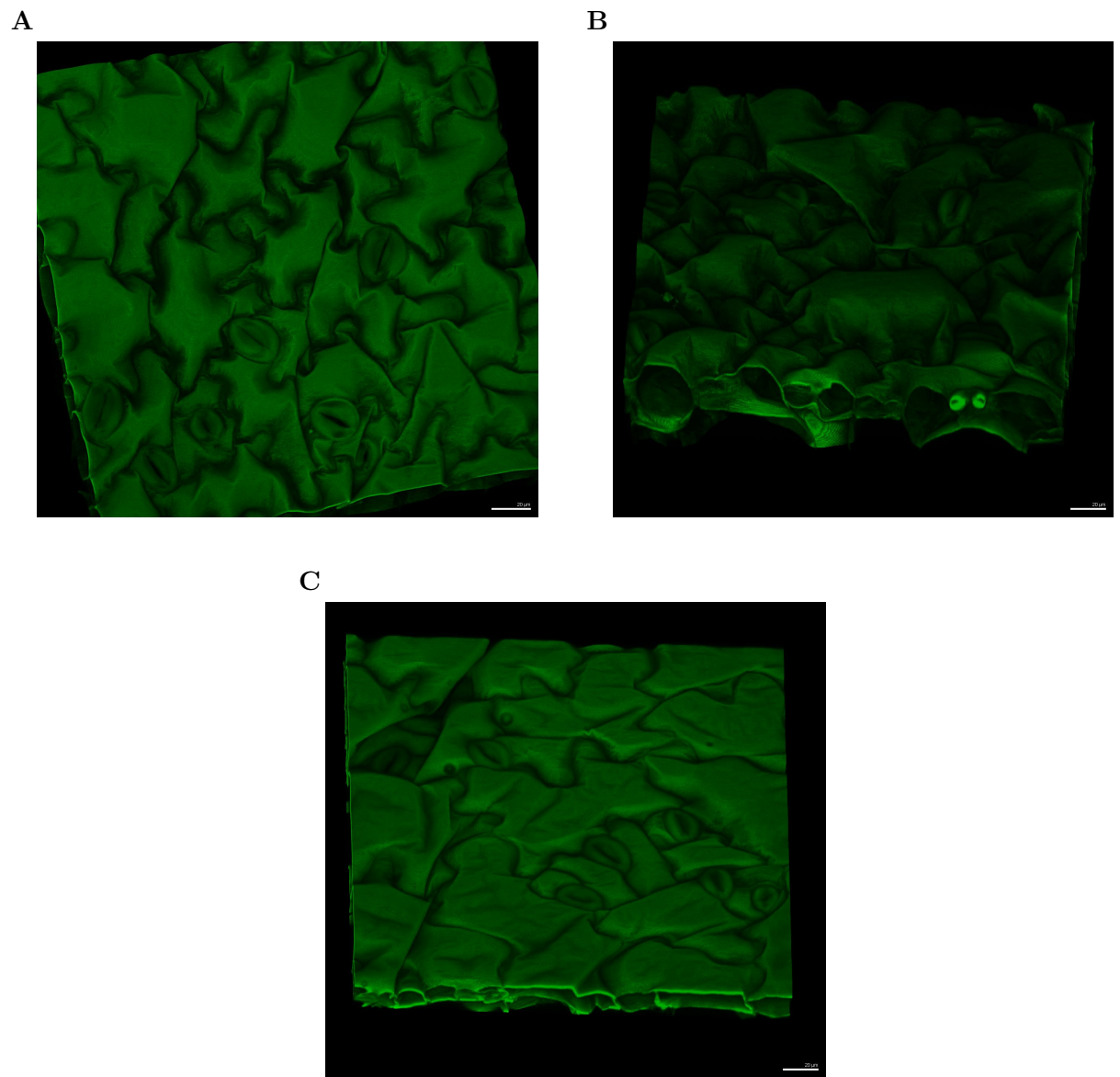


**Figure S3: Repeat of Figure 1, ten days in ClearSee.** (A) Cotyledon with nothing on top. (B) Cotyledon with slide on top. (C) Cotyledon with agar on top. Scale bars: 20  $\mu$ m.

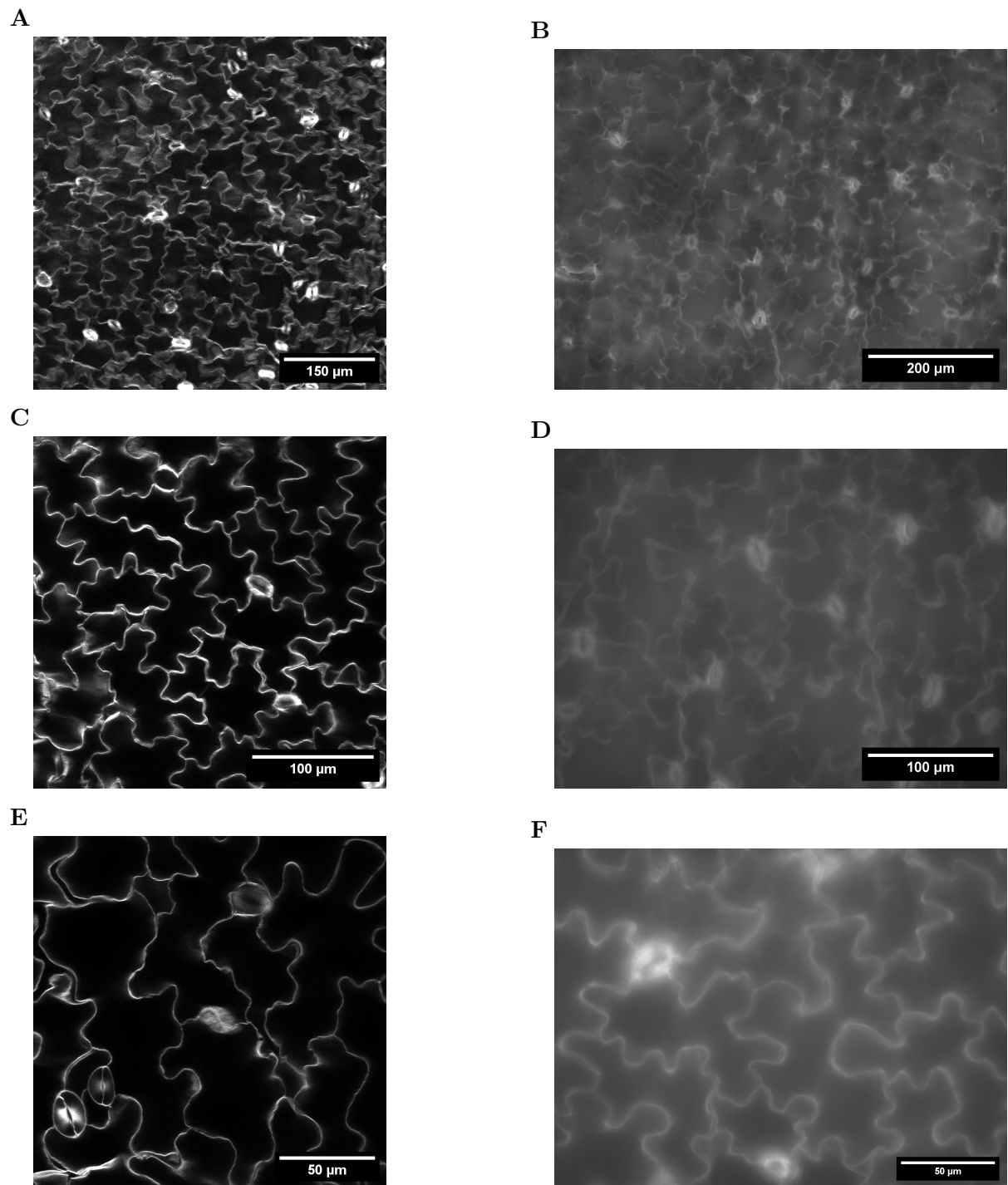


**Figure S4: Widiefield vs Confocal Calcofluor White.** All Images are taken from the same cotyledon. (A,C,E) Confocal microscopy: (A) 20x-w-cf, (A) 40x-w-cf, (A) 63x-w-cf. (B,D,F) Widefield microscopy: (B) 20x-dry-wf, (D) 40x-dry-wf, (F) 60x-oil-wf.

**Table S1: Errors for the G1T1000-workflow of different annihilations.** Counts of different error types, total number of errors (#errors), amount of cells detected by PaCeQuant segmentation (#cells) as well as the amount of errors per (corrected) cell  $e_{pc}$  for each annihilation range in  $\mu\text{m}$ .

| annih | #cells | #errors   | cut-offs | overseg | underseg | no seg | $e_{pc}$ |
|-------|--------|-----------|----------|---------|----------|--------|----------|
| 06-10 | 122    | <b>22</b> | 5        | 10      | 7        |        | 19.64%   |
| 08-10 | 116    | <b>31</b> | 24       | 5       | 2        |        | 27.93%   |
| 08-12 | 113    | <b>5</b>  | 2        | 1       | 2        |        | 4.46%    |
| 10-12 | 109    | <b>3</b>  | 1        |         | 2        |        | 2.75%    |
| 10-14 | 112    | <b>3</b>  | 1        |         | 2        |        | 2.68%    |
| 12-14 | 112    | <b>1</b>  |          |         | 1        |        | 0.89%    |
| 12-16 | 113    | <b>6</b>  | 1        | 1       | 4        |        | 5.36%    |
| 14-16 | 115    | <b>8</b>  | 2        | 2       | 4        |        | 7.08%    |

**Table S2: Errors for the G1T1000-workflow applied to six cotyledons.** Counts of different error types, total number of errors (#errors), amount of cells detected by PaCeQuant segmentation (#cells) as well as the amount of errors per (corrected) cell  $e_{pc}$  for the three annihilation ranges [ $\mu\text{m}$ ] for cotyledons 01 to 06.

| Plant | annih | #cells | #errors   | cut-offs | overseg | underseg | no seg | $e_{pc}$ |
|-------|-------|--------|-----------|----------|---------|----------|--------|----------|
| 01    | 10-12 | 109    | <b>3</b>  | 1        |         | 2        |        | 2.75%    |
|       | 10-14 | 112    | <b>3</b>  | 1        |         | 2        |        | 2.68%    |
|       | 12-14 | 112    | <b>1</b>  |          |         | 1        |        | 0.89%    |
| 02    | 10-12 | 100    | <b>12</b> | 4        | 7       | 1        |        | 12.90%   |
|       | 10-14 | 103    | <b>15</b> | 6        | 4       | 5        |        | 15.15%   |
|       | 12-14 | 97     | <b>13</b> | 4        | 6       | 3        |        | 14.29%   |
| 03    | 10-12 | 133    | <b>14</b> | 5        | 5       | 4        |        | 10.94%   |
|       | 10-14 | 135    | <b>13</b> | 6        | 5       | 2        |        | 10.00%   |
|       | 12-14 | 132    | <b>10</b> | 5        | 3       | 2        |        | 7.75%    |
| 04    | 10-12 | 90     | <b>4</b>  | 2        | 2       |          |        | 4.55%    |
|       | 10-14 | 91     | <b>2</b>  | 1        | 1       |          |        | 2.22%    |
|       | 12-14 | 91     | <b>7</b>  | 2        | 4       | 1        |        | 8.05%    |
| 05    | 10-12 | 163    | <b>2</b>  |          |         | 2        |        | 1.23%    |
|       | 10-14 | 167    | <b>6</b>  | 2        |         | 4        |        | 3.59%    |
|       | 12-14 | 168    | <b>9</b>  | 3        | 2       | 4        |        | 5.42%    |
| 06    | 10-12 | 144    | <b>12</b> | 6        | 2       | 4        |        | 8.45%    |
|       | 10-14 | 148    | <b>12</b> | 7        | 3       | 2        |        | 8.28%    |
|       | 12-14 | 146    | <b>15</b> | 7        | 5       | 3        |        | 10.64%   |

**Table S3: Errors of the fill-holes workaround of different annihilations.** Counts of different error types, total number of errors (#errors), amount of cells detected by PaCeQuant segmentation (#cells) as well as the amount of errors per (corrected) cell  $e_{pc}$  for each annihilation range in  $\mu\text{m}$ .

| annih | #cells | #errors   | cut-offs | overseg | underseg | no seg | $e_{pc}$ |
|-------|--------|-----------|----------|---------|----------|--------|----------|
| 06-10 | 115    | <b>6</b>  | 2        | 4       |          | 2      | 5.41%    |
| 08-10 | 112    | <b>4</b>  | 1        | 1       |          | 2      | 3.60%    |
| 08-12 | 112    | <b>3</b>  | 1        |         | 2        |        | 2.68%    |
| 10-12 | 108    | <b>1</b>  |          |         | 1        |        | 0.93%    |
| 10-14 | 113    | <b>4</b>  | 1        | 1       | 2        |        | 3.57%    |
| 12-14 | 114    | <b>7</b>  | 2        | 1       | 4        |        | 6.19%    |
| 12-16 | 114    | <b>7</b>  | 2        | 1       | 4        |        | 6.19%    |
| 14-16 | 113    | <b>9</b>  | 4        | 2       | 3        |        | 8.11%    |
| 14-18 | 110    | <b>13</b> | 6        | 1       | 4        | 2      | 11.93%   |
| 16-18 | 109    | <b>17</b> | 9        | 2       | 5        | 1      | 15.89%   |

**Table S4: Errors for the fill-holes workaround applied to six cotyledons.** Counts of different error types, total number of errors (#errors), amount of cells detected by PaCeQuant segmentation (#cells) as well as the amount of errors per (corrected) cell  $e_{pc}$  for the three annihilation ranges [ $\mu\text{m}$ ] for cotyledons 01 to 06.

| Plant | annih | #cells | #errors   | cut-offs | overseg | underseg | no seg | $e_{pc}$ |
|-------|-------|--------|-----------|----------|---------|----------|--------|----------|
| 01    | 08-10 | 112    | <b>4</b>  | 1        | 1       |          | 2      | 3.60%    |
|       | 08-12 | 112    | <b>3</b>  | 1        |         | 2        |        | 2.68%    |
|       | 10-12 | 108    | <b>1</b>  |          |         | 1        |        | 0.93%    |
| 02    | 08-10 | 105    | <b>8</b>  | 5        | 3       |          |        | 7.84%    |
|       | 08-12 | 107    | <b>15</b> | 6        | 6       | 3        |        | 14.85%   |
|       | 10-12 | 96     | <b>14</b> | 5        | 6       | 3        |        | 15.56%   |
| 03    | 08-10 | 139    | <b>12</b> | 3        | 4       | 4        | 1      | 8.89%    |
|       | 08-12 | 134    | <b>17</b> | 6        | 5       | 3        | 3      | 13.18%   |
|       | 10-12 | 127    | <b>13</b> | 7        | 6       |          |        | 10.74%   |
| 04    | 08-10 | 95     | <b>3</b>  | 2        | 1       |          |        | 3.19%    |
|       | 08-12 | 92     | <b>4</b>  | 1        | 1       | 2        |        | 4.40%    |
|       | 10-12 | 88     | <b>9</b>  | 1        | 5       | 3        |        | 10.84%   |
| 05    | 08-10 | 169    | <b>3</b>  | 2        |         | 1        |        | 1.78%    |
|       | 08-12 | 172    | <b>4</b>  | 1        |         | 3        |        | 2.33%    |
|       | 10-12 | 161    | <b>4</b>  | 1        |         | 3        |        | 2.48%    |
| 06    | 08-10 | 152    | <b>7</b>  | 4        | 2       | 1        |        | 4.67%    |
|       | 08-12 | 152    | <b>10</b> | 6        | 4       |          |        | 6.76%    |
|       | 10-12 | 145    | <b>9</b>  | 4        | 5       |          |        | 6.43%    |

**Table S5: Errors for the Gaussian workaround of different annihilations.** Counts of different error types, total number of errors (#errors), amount of cells detected by PaCeQuant segmentation (#cells) as well as the amount of errors per (corrected) cell  $e_{pc}$  for each annihilation range in  $\mu\text{m}$ .

| Projection | #cells | #errors   | cut-offs | overseg | underseg | no seg | $e_{pc}$ |
|------------|--------|-----------|----------|---------|----------|--------|----------|
| 08-12      | 114    | <b>20</b> | 9        | 5       | 4        | 2      | 18.35%   |
| 10-12      | 113    | <b>22</b> | 11       | 5       | 3        | 3      | 20.37%   |
| 10-14      | 114    | <b>2</b>  | 1        | 1       |          |        | 1.77%    |
| 12-14      | 113    | <b>0</b>  |          |         |          |        | 0%       |
| 12-16      | 111    | <b>2</b>  | 2        |         |          |        | 1.80%    |
| 14-16      | 111    | <b>3</b>  | 1        |         | 2        |        | 2.70%    |
| 14-18      | 113    | <b>7</b>  | 1        | 2       | 4        |        | 6.31%    |
| 16-18      | 111    | <b>10</b> | 1        | 3       | 6        |        | 9.26%    |
| 16-20      | 113    | <b>8</b>  | 1        | 1       | 6        |        | 7.14%    |
| 18-20      | 109    | <b>13</b> | 7        | 1       | 5        |        | 12.04%   |

**Table S6: Errors for the high-Gaussian workaround applied to six cotyledons.** Counts of different error types, total number of errors (#errors), amount of cells detected by PaCeQuant segmentation (#cells) as well as the amount of errors per (corrected) cell  $e_{pc}$  for the three annihilation ranges [ $\mu\text{m}$ ] for cotyledons 01 to 06.

| Plant | annih | #cells | #errors   | cut-offs | overseg | underseg | no seg | $e_{pc}$ |
|-------|-------|--------|-----------|----------|---------|----------|--------|----------|
| 01    | 10-14 | 114    | <b>2</b>  | 1        | 1       |          |        | 1.77%    |
|       | 12-14 | 113    | <b>0</b>  |          |         |          |        | 0%       |
|       | 12-16 | 111    | <b>2</b>  | 2        |         |          |        | 1.80%    |
| 02    | 10-14 | 97     | <b>6</b>  | 3        | 2       | 1        |        | 6.32%    |
|       | 12-14 | 98     | <b>10</b> | 6        | 4       |          |        | 10.64%   |
|       | 12-16 | 98     | <b>12</b> | 9        | 3       |          |        | 12.63%   |
| 03    | 10-14 | 140    | <b>15</b> | 10       | 5       |          |        | 11.11%   |
|       | 12-14 | 139    | <b>11</b> | 4        | 5       | 2        |        | 8.21%    |
|       | 12-16 | 133    | <b>11</b> | 4        | 4       | 1        |        | 8.53%    |
| 04    | 10-14 | 90     | <b>2</b>  | 1        | 1       |          |        | 2.25%    |
|       | 12-14 | 93     | <b>3</b>  |          | 3       |          |        | 3.33%    |
|       | 12-16 | 92     | <b>5</b>  | 3        | 2       |          |        | 5.56%    |
| 05    | 10-14 | 167    | <b>1</b>  | 1        |         |          |        | 0.60%    |
|       | 12-14 | 166    | <b>5</b>  | 2        |         | 2        | 1      | 3.01%    |
|       | 12-16 | 167    | <b>6</b>  | 3        | 1       |          | 2      | 3.61%    |
| 06    | 10-14 | 149    | <b>12</b> | 5        | 6       | 1        |        | 8.39%    |
|       | 12-14 | 147    | <b>9</b>  | 5        | 2       | 1        | 1      | 6.21%    |
|       | 12-16 | 144    | <b>9</b>  | 4        | 4       | 1        |        | 6.43%    |